

**The Influence of Physicochemical Parameters on Photochemical  
Internalization (PCI) Mechanism and Application of PCI as a  
Photo-Dependent RNA Delivery Strategy to Mouse Embryo**

光化学的内在化（PCI）の機構解明、およびマウス初期胚への  
RNA デリバリーへの応用

**2019, September**

**Tet Htut Soe**

**Graduate School of  
Natural Science and Technology  
(Doctor`s Course)  
OKAYAMA UNIVERSITY**

**The Influence of Physicochemical Parameters on Photochemical Internalization (PCI) Mechanism and Application of PCI as a Photo-Dependent RNA Delivery Strategy to Mouse Embryo**

A dissertation submitted by Tet Htut Soe in partial fulfilment of the requirements for the Doctor of Philosophy in Engineering in the Graduate School of Natural Science and Technology, Okayama University, Japan.

**Graduate School of  
Natural Science and Technology  
Okayama University**



**Faculty of Engineering  
3.1.1 Tsushima-Naka  
Kita-ku, Okayama 700-8530  
Japan**

**September 12, 2019**

## **CERTIFICATE**

This is to certify that Mr. Tet Htut Soe has worked on the dissertation entitled “The Influence of Physicochemical Parameters on Photochemical Internalization (PCI) Mechanism and Application of PCI as a Photo-Dependent RNA Delivery Strategy to Mouse Embryo” under my supervision. This thesis is being submitted to the Graduate School of Natural Science and Technology, Okayama University for the partial fulfillment of the requirement for the degree of Doctor of Philosophy in Engineering. It is an original record of the work conducted by the candidate and has not been submitted in full or part to any other university for the award of degree or diploma.

Takashi Ohtsuki

Takashi Ohtsuki, PhD, Professor  
Laboratory of Biomolecular Engineering  
Department of Medical Bioengineering

## Table of Contents

<b>List of Figures</b>	vii
<b>Summary</b>	1
<b>Chapter 1</b>	
<b>General Introduction</b>	
▪ Use of light in therapeutic medicine	6
▪ Role of photosensitizers in PDT and PCI	7
▪ PCI of cell penetrating peptide-photosensitizer-cargo conjugates	10
▪ Photoinduced cytosolic dispersion of RNA (PCDR) and its application	12
References	18
<b>Chapter 2</b>	
<b>The Influence of Physicochemical Parameters on Photochemical Internalization (PCI) Mechanism</b>	
Abstract	24
Introduction	25
Results and Discussion	29
• Heat (thermal mechanism) does not significantly contribute to photoinduced endosomal escape	29
• Correlation between PCI and endosomal pH	32
• Correlation between PCI and $[Ca^{2+}]_i$ increase	38
• The increased $[Ca^{2+}]_i$ mainly comes from extracellular sources	42
Conclusion	46
Materials and Methods	48
• Preparation of TatU1A-Alexa	48
• Short hairpin RNA (shRNA) preparation	48
• Cell treatment with TatU1A-PS/shRNA complexes	

and photostimulation	49
• Photo-dependent endosomal escape of the RNA under various temperatures	50
• Influence of a proton pump inhibitor on photo-dependent endosomal escape of the TatU1A-Alexa546/shRNA complex	51
• Influence of NH <sub>4</sub> <sup>+</sup> -induced increase of endosomal pH on photoinduced endosomal escape	51
• Ca <sup>2+</sup> imaging	52
References	53

### Chapter 3

#### **Application of PCI as a Photo-Dependent RNA Delivery Strategy to Mouse Embryo**

Abstract	62
Introduction	63
Results and Discussion	69
• Photoinduced RNA internalization by single cell of mouse embryo	69
• Photo-dependent knockdown of EGFP in mouse embryo	71
• Reduction of aPKC expression at apical cortex of outside cells	74
Conclusion	79
Materials and Methods	81
• Embryo collection and culture	81
• Synthetic mRNA preparation	81
• Short hairpin RNA preparation	83
• Embryo microinjection	85
• RNA delivery by PCDR method	85
• Immunofluorescence staining	86
• Quantification of fluorescence intensity	87

References	88
<b>Acknowledgements</b>	93
<b>List of Publications</b>	95
<b>Oral and Poster Presentation</b>	95

## List of Figures

Figure 1-1. Schematic illustration of cell penetrating peptide (CPP)-mediated photochemical internalization	12
Figure 1-2. Photoinduced cytosolic dispersion of RNA (PCDR)	15
Figure 1-3. Spatial regulation of specific gene expression by PCDR	16
Figure 2-1. Photoinduced endosomal escape of FAM-labeled RNA at various temperatures	31
Figure 2-2. Influence of BA1 on photoinduced cytosolic delivery of FAM-labeled RNA with TatU1A-Alexa546	33
Figure 2-3. Acid vesicles disappeared in the presence of 200 nM BA1	35
Figure 2-4. Influence of NH <sub>4</sub> Cl in the medium on photoinduced cytosolic delivery of FAM-labeled RNA	36
Figure 2-5. Acid vesicles disappeared in the presence of 10 mM NH <sub>4</sub> Cl	37
Figure 2-6. Correlation of Ca <sup>2+</sup> signal intensity with endosomal escape of the CPP-cargo-photosensitizer (TatU1A-Alexa633) at 37 °C and 4 °C	39
Figure 2-7. Correlation of Ca <sup>2+</sup> signal intensity with endosomal escape of the CPP-cargo-photosensitizer (TatU1A-Alexa546) at 37 °C and 4 °C	40
Figure 2-8. Localization of TatU1A-Alexa633 at 37 °C or 4 °C before photostimulation compared to LysoTracker Green	40
Figure 2-9. Scatter plots between cytoplasmic Alexa signal and Fluo-4 signal after photoinduced endosomal escape of TatU1A-Alexa633/shRNA (a) and TatU1A-Alexa546/shRNA (b) complexes at 37 °C	41
Figure 2-10. Cytosolic Ca <sup>2+</sup> increase during PCI depend on extracellular calcium on at 37°C or 4°C	43
Figure 2-11. Photoinduced Ca <sup>2+</sup> influx blocked by diltiazem	44
Figure 3-1. The role of Par6-aPKC polarization in early mouse embryogenesis	68
Figure 3-2. Photoinduced RNA internalization by a single cell of mouse embryos	70
Figure 3-3. EGFP silencing in mouse embryos	72
Figure 3-4. Effects of aPKC knockdown on late morula stage embryos	76
Figure 3-5. The aPKC expression was reduced at apical cortex of shaPKC injected progeny cells which were lying outside	77

## Summary

The inefficient endosomal escape of drugs or macromolecules is a major obstacle to achieving successful delivery to therapeutic targets. An efficient approach to circumvent this barrier is photochemical internalization (PCI), which uses light and photosensitizers for endosomal escape of the delivered macromolecules. PCI efficacy relies on an understanding of the endosomal escape mechanism involving the actions of photosensitizers and carrier systems used (in the case of cell penetrating peptide (CPP)-mediated PCI). It has been reported that the PCI mechanism is mainly related to photogenerated singlet oxygen, one of reactive oxygen species (ROS) generated from photoexcited sensitizers, but the mechanism is still unclear. The effect of physicochemical parameters such as heat and pH, in endosomal escape, and PCI associated changes in cells (i.e. intracellular calcium changes after photo-dependent endosomal release) are essentially needed to be clarified in mechanism of PCI.

In this study, we investigated the role of heat, pH and calcium ions in PCI-mediated endosomal escape of CPP-cargo-photosensitizer conjugate which consists of a cell permeable RNA-binding protein, TatU1A, -cargo, a shRNA, -photosensitizer (PS), Alexa546 or Alexa633. Our previous study showed that heat generated from photosensitizers does not contribute

significantly to endosomal escape. The weak evidence is that heat was not directly measured in the study. Therefore, in this study, we investigated whether heat is involved in endosomal escape of CPP-cargo-PS by changing the temperature of the cells and demonstrated that the temperature during irradiation did not significantly affect photoinduced endosomal escape efficiency of the conjugate. Since CPP-cargo-PS enter to the cells via endocytosis pathway, physiological pH condition inside the endosome may play an important role in photoinduced endosomal escape. Thus, based on our previous understanding which is endosomal pH increase the several seconds before the release of CPP-cargo-PS, we proposed that (1) endosomal pH increase, which is induced by photo-inactivation of endosomal acidifier, V-ATPase, causes the endosomal escape, or (2) the pH increase is not a cause of the endosomal escape. The results of inhibition of V-ATPase activity and endosomal pH upregulation by NH<sub>4</sub>Cl treatment indicated that PCI-mediated endosomal escape needs endosomal acidification prior to photoirradiation and supported that pH increase is not a cause of the endosomal escape but it might be due to photoinduced destabilization of the endosomal membrane.

As it has been reported that there is a mutual interplay between Ca<sup>2+</sup> and ROS signaling pathways, calcium ions might involve in the

photoinduced endosomal release of CPP-cargo-PS, which is the consequence of the ROS-induced membrane destabilization in the photosensitized cells. In this study, we found that photoinduced  $[Ca^{2+}]_i$  increase at both 4 °C (at which endocytosis was inhibited) and 37 °C conditions with TatU1A-Alexa546/shRNA, indicating that the  $[Ca^{2+}]_i$  increase is not dependent on endocytosis. Imaging of the TatU1A-PS (Alexa546 or Alexa633)/shRNA and  $Ca^{2+}$  ions during photostimulation further showed that intracellular calcium increase is not the cause of the endosomal escape of CPP-cargo-PS. By blocking voltage sensitive  $Ca^{2+}$  channel by a blocker, diltiazem, it was showed that the  $[Ca^{2+}]_i$  increase is due to photoinduced  $Ca^{2+}$  influx.

Furthermore, we have also established photoinduced cytosolic dispersion of RNA (PCDR) method to the studies of embryonic development. The differentiation of cells into inner cell mass (ICM) and trophectoderm (TE) in blastocyst stage embryos are important event that affects implantation of the embryos on mother`s uterus. This cell fate decision starts from the early 8 to 16-cell stage embryos due to the difference of cell polarity in outer and inner lying cells. As PCDR method using photoresponsive RNA carrier has an ability to control RNA function in temporal and spatial manner, introduction of RNAs into the individual cell by PCDR is a very useful

approach in the studies of cell differentiation mechanism in early embryo development. In this study, we introduced shRNA into a certain mouse embryonic cell using TatU1A-PS by photo-dependent manner and showed that PCDR is one of the promising approaches to the study of developmental process of early embryos.

# **Chapter 1**

## **General Introduction**

## **Use of light in therapeutic medicine**

Application of light in therapeutic medicine was initially studied by a number of research groups in early 1900s (1). In 1903, a physician Niels Finsen was awarded the Nobel Prize in Physiology and Medicine for his work of phototherapy in the treatment of skin tuberculosis, lupus vulgaris. Since then, the use of light application in medicine was rapidly developed as a photodynamic therapy (PDT) which has been widely studied for cancer treatment modality after discovering of hematoporphyrin derivatives (HpD), a porphyrin mixture, in tumor detection by Lipson and coworkers in 1961 (2). Later, Kelly and coworker reported the clinical application of HpD as a photosensitizer for the photodynamic destruction of human bladder carcinoma (3). As an advancement of photodynamic applications, Berg group introduced a novel mechanism which they named it as photochemical internalization (PCI) in 1999 (4). They showed endocytosed molecules, the type I RIP gelonin and horseradish peroxidase, in combination with photosensitizer, TPPS2a, can be delivered into cytosol by the light dependent manner (4). The PCI technology is based on the principles of photodynamic therapy. By exploiting photodynamic action of a photosensitizer to the light dependent endosomal membrane disruption in PCI, endocytosed molecules

can overcome the endosomal entrapment problem in therapeutic delivery approaches.

## **Role of photosensitizers in PDT and PCI**

Photosensitizers (PSs) are photosensitive compounds that produce reactive oxygen species (ROS), such as singlet oxygen ( $^1\text{O}_2$ ), when it is excited by the specific wavelength of light. After a series of photochemical reaction caused by photoexcited PS, the resultant ROS, mainly singlet oxygen, oxidize other molecules or photodamage subcellular organelle where it is located (5, 6).

Most commonly used photosensitizers in PDT are porphyrin derivatives, 1<sup>st</sup> generation PSs, such as Photofrin and Photogem. The 2<sup>nd</sup> generation PSs, such as chlorin (Temoporfin®), are improved to the higher water solubility and photo-adsorption coefficient (6). The third generation PSs, which are photosensitizer conjugates by conjugating the PS with targeting components, have been obtained high specific localization to the tumor sites (7). For instance, PS conjugated with an antibody which directs against the tumor antigens showed significant strong antitumor effects and tumor localization (7, 8).

Localization of PSs play a big role in photoinduced tissue damage of PDT because  $^1\text{O}_2$  has a short lifetime ( $<0.04$  microsecond) and can migrate less than  $0.02 \mu\text{m}$  after its formation (9, 10). Photosensitizers also differ from each other according to their localization selectivity. For example, hydrophilic PSs localize in endosome or lysosome, the lysyl chlorin p6 for lysosomes, the monocationic porphyrin and the porphycene monomer localize in membranes and mitochondria (11). Besides localization of PS, the photophysical properties are important for photoinduced membrane damage in which singlet oxygen mainly involved. An efficient photosensitizer should have following photophysical properties : (1) high absorption coefficient; (2) a triplet state of appropriate energy ( $E_T \geq 95 \text{ kJ mol}^{-1}$ ) which is efficiently transfer energy to ground state oxygen; (3) high quantum yield ( $\phi_T \geq 0.4$ ) and long lifetimes ( $\tau_T > 1 \mu\text{s}$ ) of the triplet state ; and (4) high photostability (5). For instance, the first generation PS, hematoporphyrin has a moderate absorption band at 630 nm with high  $^1\text{O}_2$  quantum yield ( $\phi_\Delta = 0.65$  in an organic solvent) and Al phthalocyanine-tetra-sulfonic acid has a strong absorption band at 673 nm and produce  $^1\text{O}_2$  yield at 0.38 (in water) (5).

As described above, PCI mechanism is dependent on photodynamic action of PS that trigger endosomal escape of targeted molecules. Thus,

photosensitizers which are used in PCI need to have endosomal localization ability with a suitable physico-chemical and photophysical properties to achieve the optimal PCI (12). Most commonly used photosensitizer in PCI are porphyrin/chlorin photosensitizers such as meso-tetraphenyl porphyrin disulphonate (TPPS2a) and tetra (4-sulfonatophenyl) porphine (TPPS4), disulfonated aluminum phthalocyanine (AlPcS2a), and disulfonated tetraphenyl chlorin (TPCS2a). Recently, our group has studied the relationship of endosomal escape of cargo molecule to the photophysical properties of some dyes. From the study, we understood that photoinduced endosomal escape of cargo was dependent on the  $^1\text{O}_2$  generation from the dye which was covalently attached to a cell penetrating peptide (CPP). We also found that not only high  $^1\text{O}_2$  quantum yield photosensitizer, such as Rose Bengal ( $\phi_{\Delta} = 0.86$  in EtOH), but also weak  $^1\text{O}_2$  quantum yield photosensitizers, such as Alexa594 ( $\phi_{\Delta} = 0.028$  in octanol) and Alexa633 ( $\phi_{\Delta} = 0.043$  in octanol), sufficiently rendered an efficient endosomal escape (13). Therefore, in this study, we used weak  $^1\text{O}_2$  quantum yield photosensitizers, Alexa 546 and Alexa633, by conjugating with a CPP.

## **PCI of cell penetrating peptide-photosensitizer-cargo conjugates**

The cellular transduction activity of cationic peptides enables to be used as a carrier in the intracellular delivery of cell-impermeable macromolecules, such as nucleic acids, proteins and drugs (14). To date, several peptides have been developed as a CPP such as HIV-1 TAT transactivation protein, antennapedia from Antennapedia homeodomain, transportan and synthetic arginine rich-peptides (eg. R9 peptide) (14,15). Since CPP can fuse or conjugate with fluorophores or fluorescence dyes, CPP-photosensitizer conjugates have been applied in the light dependent delivery of macromolecules (16, 17). A significant PCI efficacy was observed in HN5 carcinoma cells when Tat peptide-tetraphenyl porphyrin conjugate and a protein toxin, saporin, were used (17). While applying a fluorophore, 5,6-carboxy-tetramethylrhodamine (TMR) and R9 peptide or TAT peptide in PCI, not photosensitizer alone but also CPP involvement in destabilization of membrane due to photodamage of membrane lipids, could synergistically enhance photolytic endosomal release (16,18).

We have developed a CPP photosensitizer conjugate which includes a cell penetrating peptide, HIV-1 TAT (-YGRKKRRQRRR-) genetically fused with a small RNA binding domain (RBD), 98 amino acid at its N-

terminus, of U1 small nuclear ribonucleoprotein A (U1A) and a fluorescent dye. The TatU1A binds the fluorescence dye by reacting its thiol group with a maleimide group of the dye. The CPP photosensitizer conjugate, TatU1A-PS, can noncovalently bind with biological active molecules, such as siRNA bearing U1A RBD binding sequence (19) (Fig. 1-2a). The cargo, siRNA, is needed to be designed as a shRNA structure by adding U1A RBD binding sequence in its loop region. The TatU1A-PS cargo complexes are endocytosed and trapped inside the endosomes until they are exposed to specific wavelength of light (Fig. 1-1). The oxidative damage of membrane phospholipids by singlet oxygen induction from the reaction of photoexcited PS and molecular oxygen can cause endosomal membrane destabilization. After the photoinduced destabilization of endosomal membrane, the endocytosed complexes are released to the cytosol and actively start their targeted functions. But, the molecular details of the endosomal escape are still unknown in PCI mechanism. Based on our previous understanding of it, e.g. endosomal pH increase was found prior to photoinduced endosomal escape of CPP-PS/shRNA (13), a number of physicochemical parameters might have an influence on photoinduced endosomal escape. Thus, we investigated the relation of PCI to some physicochemical parameters in this study. The findings of our study are described at Chapter 2.

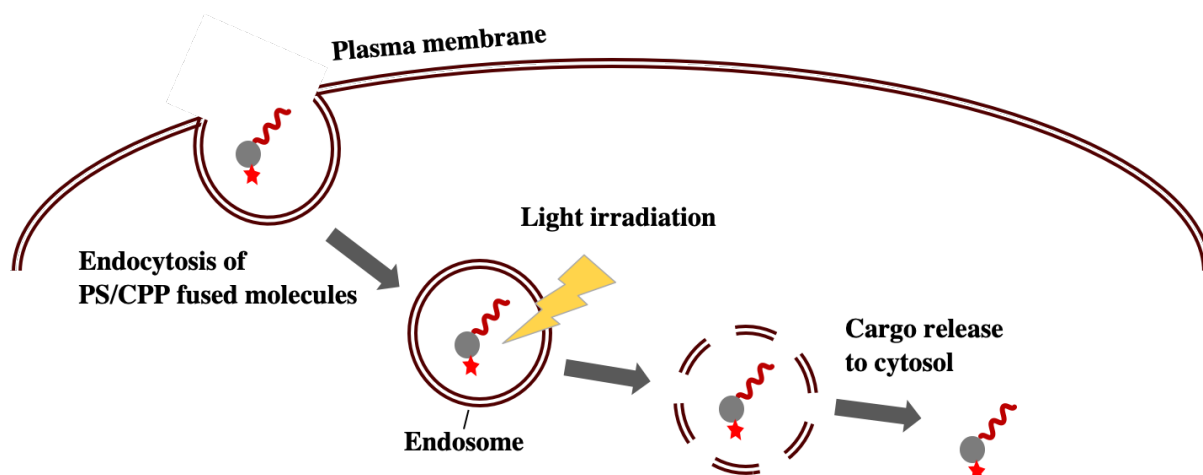


**Figure 1-1.** Schematic illustration of cell penetrating peptide (CPP)-mediated photochemical internalization.

## **Photoinduced cytosolic dispersion of RNA (PCDR) and its application**

Applying PCI mechanism, we have developed a light-directed RNA delivery method by using photosensitive RNA carrier (20). This method is named as photoinduced cytosolic dispersion of RNA (PCDR) (Fig. 1-2). In this method, cells are incubated with TatU1A-PS/RNA complex about 2-3 h in order to occur cellular internalization (Fig. 1-2b). While the complex is entrapped in endosomes, light is used to disrupt endosomal membrane and then RNA was dispersed to cytosol. This endosomal escape occurs within a

few second to a few minutes after irradiating by a suitable light energy (e.g. 10 or 20 J/ cm<sup>2</sup>) with appropriate wavelength to PS.

Light controllable RNA carrier in PCDR is a very useful for the studies of complex cellular activities such as cellular differentiation and cell proliferation process. Moreover, spatial and temporal control of small RNAs, e.g. controlled release of siRNA for RNAi mediated mechanism, is also a beneficial approach for the precise regulation of gene functions in these cellular processes. Our group have studied photopatterned RNAi mediated gene silencing and single cell RNAi, showing spatial gene regulation in mammalian cell by PCDR (21). In that study, photopatterned EGFP silencing was performed by light irradiation to the TatU1A-Alexa633 treated dEGFP-CHO (CHO cell continuously expressing EGFP) through photomask (Fig. 1-3a). Laser light induced gene silencing in single cell without causing cellular damages was also demonstrated (Fig. 1-3b).

RNA can be introduced into cytosol with rapid delivery and low cytotoxicity via photoinduced endosomal escape by PCDR method (22). One great benefit of PCDR is the repeated introduction of RNAs or the introduction of two different RNAs in short intervals (< 4 h) by using two photosensitizers. For example, sequential knockdown of mOrange2 and GFP by red light induced introduction of TatU1A-Alexa633/shmOrange and NIR

induced introduction of TatU1A-DY750/shGFP (22). Recently, our group has reported that significant increase in apoptotic activity after photoirradiation while TatBim peptide-photosensitizer (a CPP-PS as a RNA carrier with apoptotic activity) and a miRNA (miR-34a) which induces apoptosis were administered by PCDR (23). A number of research groups have also studied that light-controlled delivery of RNA molecules to the targeted functions: Oliveira and coworkers have shown that PCI enhanced the silencing of epidermal growth factor receptor (EGFR) by using PSs, TPPS2a in vitro and AlPcS2a in vivo with anti-EGFR siRNA lipoplex (24, 25). Moreover, Raemdonck and coworkers have demonstrated that PCI mediated delivery of siRNA-loaded dex-HEMA-co-TMAEMA nanogels can significantly improve silencing of luciferase gene expression as compared to non-PCI treated siRNA loaded nanogel (26). Boe and coworker have also reported that light induced exogenous gene expression in a human osteosarcoma cell line by the delivery of EGFP mRNA molecules in PCI manner, indicating that a potential strategy for the time- and site- specific control in protein production (27).

Other physical introduction methods such as microinjection and electroporation can introduce RNAs rapidly in general. However, they have low transfection efficiency in some cell types such as neuronal cell (28) and

may cause cell damages, particularly in the case of multiple RNAs introduction. Commonly used chemical transfection methods, such as lipofection, have the limitation in the study of temporal and spatial RNA functions and rapid control of cellular events.

All the facts described above proved that application of PCI as a photo-dependent RNA delivery is a promising approach to regional specific gene regulation in cells. Therefore, we planned to apply this strategy to the studies of mammalian embryogenesis in which transcriptional and polarity regulators are spatially involved in cellular differentiation of early embryo. The details of this study are described at Chapter 3.

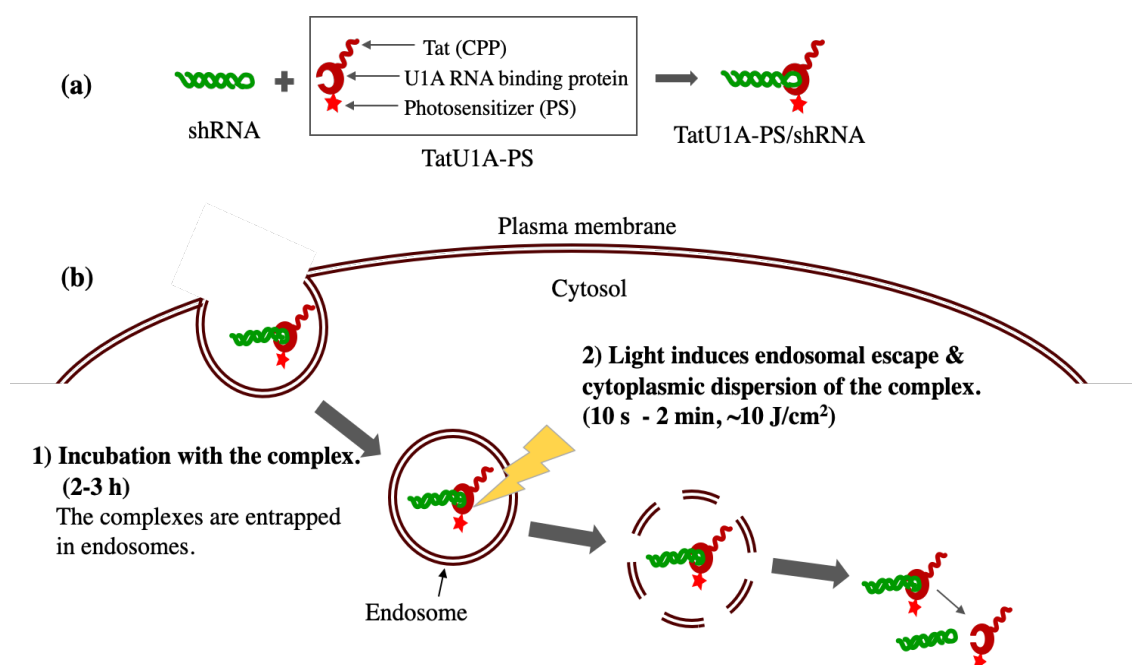


**Figure 1-2.** Photoinduced cytosolic dispersion of RNA (PCDR): (a) Structural diagrams of TatU1A-PS and TatU1A-PS/shRNA complex. (b) Schematic illustration of the endosomal escape of CPP-shRNA-photosensitizer conjugate.

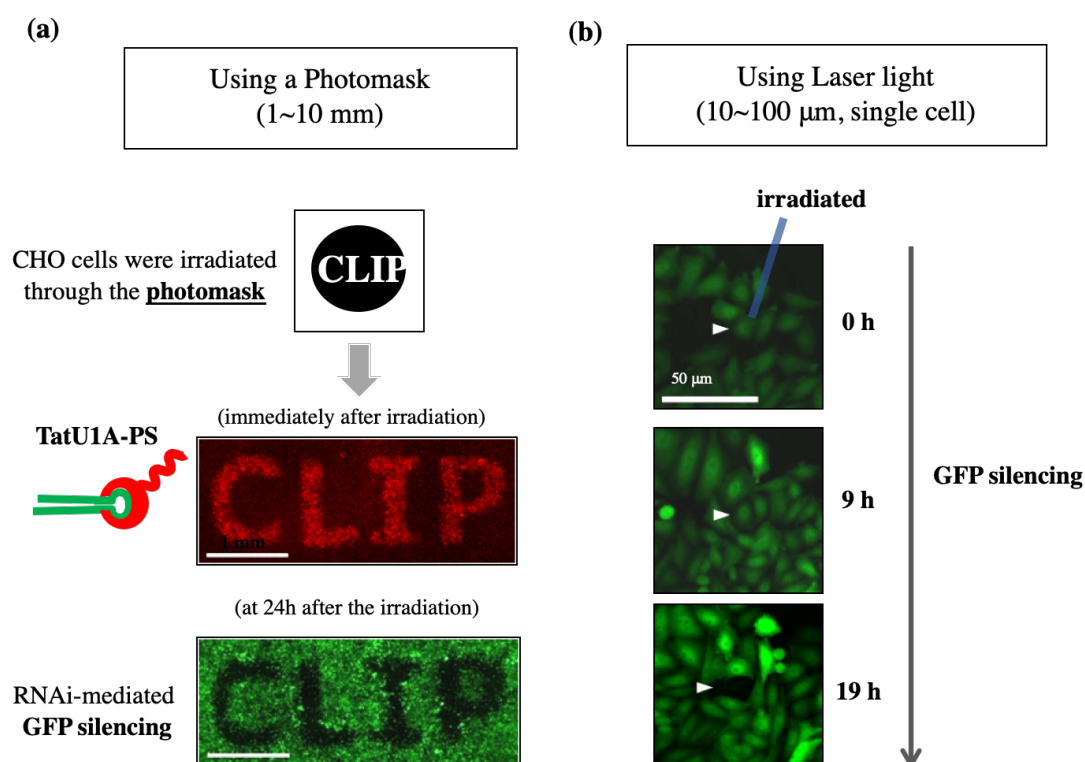


**Figure 1-3.** Spatial regulation of specific gene expression by PCDR. (a) Photoinduced RNAi mediated EGFP silencing through photomask. Cells were irradiated through the photomask. Immediately after irradiation, TatU1A-PS and RNA dispersed within cytosol. At 24h after irradiation, RNAi mediated GFP silencing was observed only in the irradiated area. (b) Single-cell RNAi by laser irradiation. A single dEGFP-CHO cell, indicated

by an arrowhead, was irradiated by a laser at 635 nm. At 19 h after irradiation, GFP silencing occurred only in the irradiated single cell (21).

## References

1. MacDonald IJ, Dougherty TJ. Basic principles of photodynamic therapy. *J. Porphyrins and Phthalocyanines*. 2001; 5: 105-129.  
doi:10.1002/jpp.328
2. Lipson RL, Baldes EJ, Olsen AM. The use of a derivative of hematoporphyrin in tumor detection. *J Natl Cancer Inst*. 1961; 26: 1-11. doi:10.1093/jnci/26.1.1
3. Kelly JF, Snell ME, Berenbauai MC. Photodynamic destruction of human bladder carcinoma. *Br J Cancer*. 1975; 31(2): 237-244.  
doi:10.1038/bjc.1975.30
4. Berg K, Selbo PK, Prasmickaite L, et al. Photochemical internalization: A novel technology for delivery of macromolecules into cytosol. *Cancer Res*. 1999; 59(6): 1180-1183.
5. DeRosa MC, Crutchley RJ. Photosensitized singlet oxygen and its applications. *Coord Chem Rev*. 2002; 233–234:351-371.  
doi:10.1016/S0010-8545(02)00034-6
6. Bae BC, Na K. Development of polymeric cargo for delivery of photosensitizer in photodynamic therapy. *Int J Photoenergy*. 2012.  
doi:10.1155/2012/431975
7. Josefsen LB, Boyle RW. Photodynamic therapy: Novel third-

- generation photosensitizers one step closer? *Br J Pharmacol*. 2008.  
154(1):1-3 doi:10.1038/bjp.2008.98
8. Kataoka H, Nishie H, Hayashi N, et al. New photodynamic therapy with next-generation photosensitizers. *Ann Transl Med*. 2017.  
doi:10.21037/atm.2017.03.59
  9. Moan J, Berg k. the photodegradation of porphyrins in cells can be used to estimate the lifetime of singlet oxygen. *Photochem Photobiol*. 1991. doi:10.1111/j.1751-1097.1991.tb03669.x
  10. Peng Q, Moan J, Nesland JM. Correlation of subcellular and intratumoral photosensitizer localization with ultrastructural features after photodynamic therapy. *Ultrastruct Pathol*. 1996.  
doi:10.3109/01913129609016306
  11. Dougherty T., Gomer C., Henderson B., Jori G., Kessel D., Korbek M., Moan J. PQPT. Review - Photodynamic therapy. *J Natl Cancer Inst*. 1998.
  12. Berg K, Nordstrand S, Selbo PK, Tran DTT, Angell-Petersen E, Høgset A. Disulfonated tetraphenyl chlorin (TPCS 2a), a novel photosensitizer developed for clinical utilization of photochemical internalization. *Photochem Photobiol Sci*. 2011.  
doi:10.1039/c1pp05128h

13. Ohtsuki T, Miki S, Kobayashi S, et al. The molecular mechanism of photochemical internalization of cell penetrating peptide-cargo-photosensitizer conjugates. *Sci Rep.* 2015; 5. doi:10.1038/srep18577
14. Erazo-Oliveras A, Muthukrishnan N, Baker R, Wang TY, Pellois JP. Improving the endosomal escape of cell-penetrating peptides and their cargos: Strategies and challenges. *Pharmaceuticals.* 2012;5(11):1177-1209. doi:10.3390/ph5111177
15. Jones SW, Christison R, Bundell K, et al. Characterisation of cell-penetrating peptide-mediated peptide delivery. *Br J Pharmacol.* 2005. doi:10.1038/sj.bjp.0706279
16. Muthukrishnan N, Johnson GA, Erazo-Oliveras A, Pellois JP. Synergy between cell-penetrating peptides and singlet oxygen generators leads to efficient photolysis of membranes. *Photochem Photobiol.* 2013; 89(3): 625-630. doi:10.1111/php.12036
17. Wang JTW, Giuntini F, Eggleston IM, Bown SG, MacRobert AJ. Photochemical internalisation of a macromolecular protein toxin using a cell penetrating peptide-photosensitiser conjugate. *J Control Release.* 2012; 157(2): 305-313. doi:10.1016/j.jconrel.2011.08.025
18. Meerovich I, Muthukrishnan N, Johnson GA, Erazo-Oliveras A, Pellois JP. Photodamage of lipid bilayers by irradiation of a

- fluorescently labeled cell-penetrating peptide. *Biochim Biophys Acta - Gen Subj*. 2014; 1840(1): 507-515. doi:10.1016/j.bbagen.2013.10.011
19. Endoh T, Sisido M, Ohtsuki T. Cellular siRNA delivery mediated by a cell-permeant RNA-binding protein and photoinduced RNA interference. *Bioconjug Chem*. 2008; 19(5): 1017-1024. doi:10.1021/bc800020n
  20. Matsushita-Ishiodori Y, Kuwabara R, Sakakoshi H, Endoh T, Ohtsuki T. Photosensitizing carrier proteins for photoinducible RNA interference. *Bioconjug Chem*. 2011; 22(11): 2222-2226. doi:10.1021/bc200095a
  21. Endoh T, Sisido M, Ohtsuki T. Spatial regulation of specific gene expression through photoactivation of RNAi. *J Control Release*. 2009;137(3):241-245. doi:10.1016/j.jconrel.2009.04.015
  22. Shiraga K, Soe TH, Matsumoto S, Watanabe K, Ohtsuki T. Red and Near-Infrared Light-Directed Cytosolic Delivery of Two Different RNAs Using Photosensitive RNA Carriers. *Bioconjug Chem*. 2018;29(9):3174-3179. doi:10.1021/acs.bioconjchem.8b00487
  23. Kim H, Kitamatsu M, Ohtsuki T. Combined apoptotic effects of peptide and miRNA in a peptide/miRNA nanocomplex. *J Biosci Bioeng*. 2019. doi:10.1016/j.jbiosc.2019.01.003

24. Oliveira S, Fretz MM, Høgset A, Storm G, Schiffelers RM. Photochemical internalization enhances silencing of epidermal growth factor receptor through improved endosomal escape of siRNA. *Biochim Biophys Acta - Biomembr.* 2007. doi:10.1016/j.bbamem.2007.01.013
25. Oliveira S, Hogset A, Storm G. Delivery of siRNA to the Target Cell Cytoplasm: Photochemical Internalization Facilitates Endosomal Escape and Improves Silencing Efficiency, In Vitro and In Vivo. *Curr Pharm Des.* 2008;14(34):3686-3697. doi:10.2174/138161208786898789
26. Raemdonck K, Naeye B, Buyens K, et al. Biodegradable dextran nanogels for RNA interference: Focusing on endosomal escape and intracellular siRNA delivery. *Adv Funct Mater.* 2009. doi:10.1002/adfm.200801795
27. Bøe S, Sæbøe-Larssen S, Hovig E. Light-Induced Gene Expression Using Messenger RNA Molecules. *Oligonucleotides.* 2009. doi:10.1089/oli.2009.0209
28. Zeitelhofer M, Vessey JP, Xie Y, Tubing F, Thomas S, Dahm R. High-efficiency transfection of mammalian neurons via nucleofection. *Nat Protoc.* 2007. doi:10.1038/nprot.2007.226

## **Chapter 2**

### **The Influence of Physicochemical Parameters on Photochemical Internalization (PCI) Mechanism**

## Abstract

The inefficient endosomal escape of drugs or macromolecules is a major obstacle to achieving successful delivery to therapeutic targets. An efficient approach to circumvent this barrier is photochemical internalization (PCI), which uses light and photosensitizers for endosomal escape of the delivered macromolecules. The PCI mechanism is related to photogenerated singlet oxygen, but the mechanism is still unclear. In this study, we examined the relation of PCI to heat, pH and  $\text{Ca}^{2+}$  ions using cell penetrating peptide (CPP)-cargo-photosensitizer (Alexa546 or Alexa633) conjugates. A cell temperature changing experiment demonstrated that heat (thermal mechanism) does not significantly contribute to the photoinduced endosomal escape. Inhibition of V-ATPase proton pump activity and endosomal pH upregulation indicated that PCI-mediated endosomal escape needs endosomal acidification prior to photoirradiation. Imaging of the CPP-cargo-photosensitizer and  $\text{Ca}^{2+}$  ions during photostimulation showed that intracellular calcium increase is not the cause of the endosomal escape of the complex. The increment is mainly due to  $\text{Ca}^{2+}$  influx. These findings show the importance of extra- and intracellular milieu conditions in the PCI mechanism and enrich our understanding of PCI-related changes in cell.

## Introduction

Endosomal entrapment is a major problem in intracellular macromolecule delivery methods depending on the endocytic pathway. Photochemical internalization (PCI) is an efficient strategy for the endosomal escape of the delivered molecules that uses light and photosensitizers. (1–3). PCI-mediated delivery of macromolecules like proteins and nucleic acids *in vitro* or *in vivo* has been widely used and discussed by many research groups. (4–7). PCI efficacy relies on an understanding of the endosomal escape mechanism involving the actions of photosensitizers and carrier systems used.

The cell penetrating peptide (CPP)-cargo-photosensitizer conjugate used in this study includes a TAT CPP, U1A RNA binding protein and a photosensitizer (TatU1A-PS), and an shRNA as a cargo (8–11). Alexa Fluor 546 (Alexa546) and Alexa Fluor 633 (Alexa633) were attached to the TatU1A protein to act as photosensitizers. The TatU1A-PS/shRNA complex enters the cells via endocytosis. However, endosomal entrapment of cargo molecules hinders its efficient cytosolic delivery until light irradiation. The entrapped endocytosed CPP-cargo-photosensitizer conjugate can pass through the endosomal membrane via the PCI mechanism using light irradiation of the photosensitizer. Several reports showed that the endosomal

membrane is destabilized due to oxidation by reactive oxygen species (ROS), especially singlet oxygen ( $^1\text{O}_2$ ), which can induce lipid peroxidation of membrane unsaturated lipids, glycolipids and cholesterol (12–14). We previously discussed the endosomal release of TatU1A-PS/shRNA by focusing on various photophysical parameters of photosensitizers, including photogenerated  $^1\text{O}_2$ , fluorescence, and heat from weak  $^1\text{O}_2$  quantum yield photosensitizers, such as Alexa633 and Alexa594 (15). We indicated that endosomal escape efficiencies are mainly related to photogenerated  $^1\text{O}_2$ , not heat, from photosensitizers. In addition, we discovered an endosomal pH increase before the photoinduced endosomal escape (15). However, our previous report lacks detailed explanations of how these factors are directly related to endosomal escape. To better understand the CPP mediated PCI mechanism, it is essential to consider what other factors might influence endosomal escape efficiencies during PCI.

Physiological pH change associated with endosomal maturation plays an important role in endo-lysosomal trafficking and endosomal escape of some enveloped viruses and protein toxins (16,17). During endosomal maturation, endosomes are acidified (from pH about 6.5 of early to pH about 5.5 of late endosome) (16–18). The acidification relates to the endosomal trafficking of foreign molecules; for example, low endosomal pH is related

to the endosomal release of flock house virus into the cytosol (19). The vacuolar H<sup>+</sup> ATPase (V-ATPase) maintains acidic conditions in endocytosis organelles by translocating protons across the membrane (20,21). This V-ATPase is highly sensitive to an inhibitor, bafilomycin A1 (BA1), which regulates endosomal pH, and affects endosomal trafficking and maturation (21–23). In our previous study using CPP-cargo-photosensitizer (TatU1A-PS/shRNA) conjugate (15), we observed a pH increase inside the endosome after photoirradiation. Thus, endosomal pH may be related to PCI-mediated cargo release from endosomes. However, we do not know how pH affects light-dependent endosomal escape of cargoes.

Calcium ions might be another crucial factor triggering the ROS-induced endosomal destabilization in the photosensitized cells as some studies reported a mutual interplay between Ca<sup>2+</sup> and ROS signaling pathways and photoinduced increase of cytoplasmic calcium ion concentration ([Ca<sup>2+</sup>]<sub>i</sub>) in the presence of photosensitizers (24–26). The source of the increased [Ca<sup>2+</sup>]<sub>i</sub> is still debated (25). Some studies indicate that Ca<sup>2+</sup> influx is the main source (26–28). Others claim that the release from internal Ca<sup>2+</sup> stores, like the endoplasmic reticulum (ER), endosomes and mitochondria, plays a large role in the [Ca<sup>2+</sup>]<sub>i</sub> increase (29-31). In the case of the CPP-photosensitizer conjugate, carboxytetramethylrhodamine-labeled

TAT peptide (TMR-TAT)-mediated PCI was accompanied by a  $[Ca^{2+}]_i$  increase, which is thought to be due to endosomal  $Ca^{2+}$  release (32). Therefore, it would be interesting to know how the  $[Ca^{2+}]_i$  increase after photosensitization relates to PCI with our CPP-cargo-photosensitizer conjugate.

In this study, we fill in gaps in our previous understanding of endosomal escape of the CPP-cargo-photosensitizer conjugate (TatU1A-PS/shRNA) by focusing on the roles of heat, pH and  $Ca^{2+}$ . A study recently concluded that photogenerated heat from photosensitizers is not significantly correlated with endosomal escape by focusing on photophysical parameters of photosensitizers (15). In this study, we investigated the involvement of heat in endosomal escape of TatU1A-PS/shRNA by changing the temperature of the cell just before photoirradiation. The correlation of PCI and endosomal pH was investigated under two hypotheses to reveal the underlying mechanism of pH increase after photostimulation. In addition, we examined whether the  $[Ca^{2+}]_i$  increase after photoirradiation is related to endosomal escape of TatU1A-PS/shRNA.

## **Results and Discussion**

### **Heat (thermal mechanism) does not significantly contribute to photoinduced endosomal escape**

The mechanism of photoinduced endosomal escape is reportedly based on endosomal membrane destabilization by photogenerated  $^1\text{O}_2$  from photosensitizers or photogenerated heat from photothermal agents (e.g., gold nanoparticles and graphene nanosheets) that can convert photon energy to vibrational energy (33). To know the contribution of photogenerated  $^1\text{O}_2$  and heat to endosomal escape by TatU1A-PS, we previously investigated the correlation between photophysical parameters of multiple photosensitizers and the endosome escape efficiency of TatU1A-PS/shRNA (15). The previous study showed that photogenerated  $^1\text{O}_2$  from photosensitizers is highly associated with endosomal escape efficiencies and that heat generated from photosensitizers does not contribute significantly to endosomal escape. Although heat was not directly measured in the previous study, we discussed using photogenerated heat estimated using fluorescence and  $^1\text{O}_2$  quantum yields of each photosensitizer. Thus, the conclusion that heat is not relevant to endosomal escape is only supported by weak evidence.

Therefore, we investigated whether heat is involved in endosomal escape of CPP-cargo-photosensitizer (TatU1A-Alexa546/shRNA) by changing the temperature of the cells. To exclude the influence of temperature on endocytosis, the cells were incubated for 2 h at 37°C with TatU1A-Alexa546 and the RNA, and we only changed the temperature immediately before and during photoirradiation. Cells were irradiated at 10, 20 or 30 °C, in contrast to the normal protocol at room temperature around 20-25 °C. If photoinduced endosomal escape depends on the photothermal effect generated by TatU1A-Alexa546, temperature change would significantly affect the endosomal escape efficiency. As a result, there was no significant difference in the endosomal escape efficiency at any temperature from 10 to 30 °C (Fig. 2-1). Therefore, we confirmed that heat does not significantly contribute to photoinduced endosomal escape.

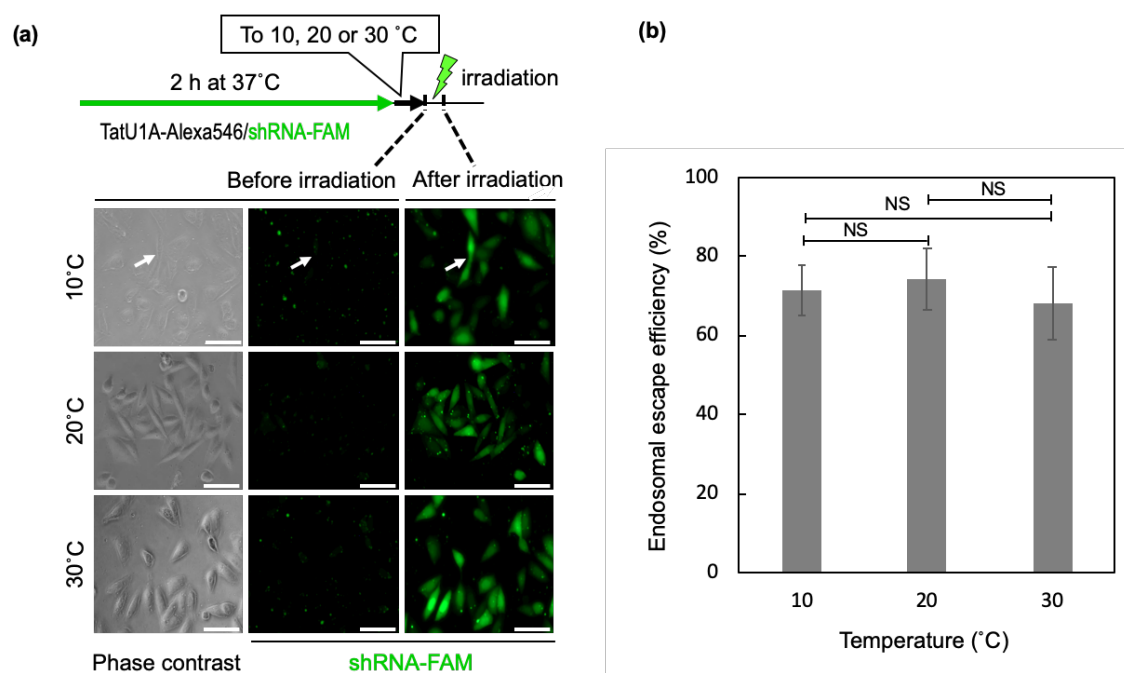


**Figure 2-1.** Photoinduced endosomal escape of FAM-labeled RNA at various temperatures. TatU1A-Alexa546 was used as a RNA carrier and photosensitizer. **(a)** Phase contrast and FAM fluorescence images before and after irradiation. The arrows indicate a representative cell before and after endosomal escape of FAM-labeled RNA. Scale bars indicate 50  $\mu$ m. **(b)** Endosomal escape efficiencies of FAM-labeled RNA at various temperatures. Data are shown as the mean  $\pm$  SEM (n = 5; each of the analyzed areas included 48 cells on average). The statistical analysis was performed by one-way ANOVA with Tukey`s multiple comparison test. (NS= mean not significantly different from 10°C vs. 20°C, 10°C vs. 30 °C and 20°C vs. 30°C =  $P > 0.05$ ). A P-values with less than 0.05 was considered to be statistically significant.

## Correlation between PCI and endosomal pH

In our previous study, endosomal pH increase was observed after light irradiation and 60–80 s before the endosomal escape of the TatU1A-photosensitizer/RNA complex (15). The photoinduced pH increase may be due to (1)  $^1\text{O}_2$ -induced inactivation of the endosomal V-ATPase proton pump responsible for the pH decrease, or (2) leakage of endosomal protons into the cytoplasm caused by  $^1\text{O}_2$ -induced destabilization of the endosomal membrane. Based on these two possibilities, we made two hypotheses about the relationship between pH increase and endosomal escape. (I) Endosomal pH increase, which is induced by V-ATPase inactivation, causes the endosomal escape, or (II) the pH increase is not a cause of the endosomal escape, but a result of photoinduced destabilization of the endosomal membrane.

To test hypothesis (I), we investigated the influence of bafilomycin A1 (BA1), an inhibitor of V-ATPase (21,22,34). Even after cellular treatment with 200 nM BA1 for 30 min, endosomal pH increased from ~6 to ~7 (35). Thus, our conditions for cellular treatment (200 nM BA1 for 1-2 h, Fig. 2-2a) are thought to induce V-ATPase inactivation and endosomal pH increase. As a result, BA1 addition to the cells did not induce endosomal escape of TatU1A-Alexa546/shRNA (Fig. 2-2b “Before” images). If

hypothesis (I) is valid, BA1 induces V-ATPase inactivation and endosomal escape of TatU1A-Alexa546/shRNA. Therefore, hypothesis (I) was rejected. BA1 addition to the cells did not significantly disturb endosomal accumulation of the TatU1A-Alexa546/shRNA complex, but photoinduced endosomal escape of the complex was inhibited (Fig. 2-2b “After” images, and Fig. 2-2c). This suggests that the active proton pump is necessary for photoinduced endosomal escape, which argues against hypothesis (I).

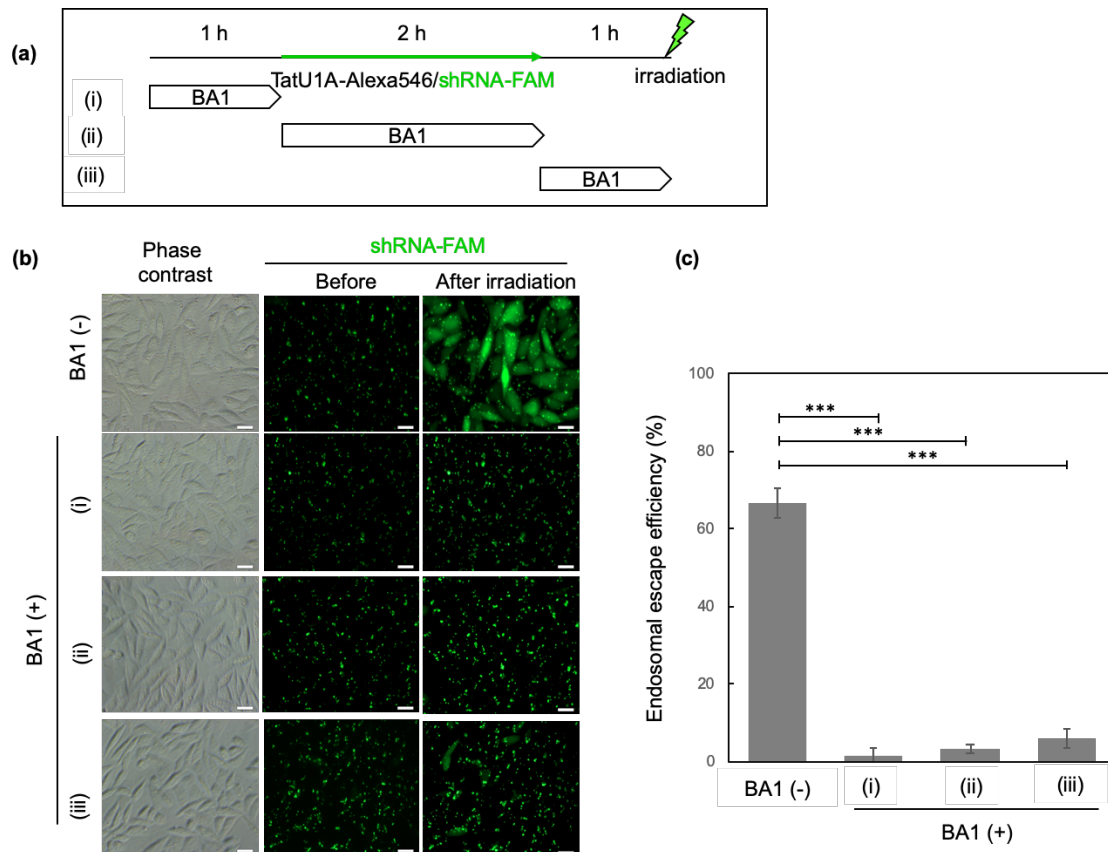


**Figure 2-2.** Influence of BA1 on photoinduced cytosolic delivery of FAM-labeled RNA with TatU1A-Alexa546. **(a)** Timing of BA1 addition: (i) before treatment with the complex (1 h) (ii) at the same time as treatment with the

complex (2 h), or (iii) after treatment with the complex (1 h). **(b)** FAM fluorescence images before and after irradiation. The BA1 addition timings (i, ii, and iii) are as shown in (a). Scale bars indicate 20  $\mu\text{m}$ . **(c)** Influence of BA1 on endosomal escape efficiency. Data are shown as the mean  $\pm$  SEM ( $n = 4$ ; each of the analyzed areas included 82 cells on average). The statistical significance in mean values was determined using one-way ANOVA with Dunnett's multiple comparison test using BA1(-) as a control (\*\*\*)  $P < 0.0001$ ). A P-values with less than 0.05 was considered to be statistically significant.

Almost no acidic vesicles were observed when the cells were treated with BA1 (Fig. 2-3), indicating the inhibition of endosomal acidification rather than the absence of endosomal vesicles since the vesicles were observed in FAM (Fig. 2-2b) and Alexa546 (Fig. 2-3) images. Inhibition of endosomal acidification by BA1 resulted in the inhibition of photoinduced endosomal escape (Fig. 2-2b "After" images, and Fig. 2-2c). These results indicate that PCI-mediated endosomal escape needs endosomal acidification prior to photoirradiation. This supports hypothesis (II) that endosomal pH increase is not the cause of endosomal escape. The photoinduced endosomal pH increase (15) might be a phenomenon associated with light- and photosensitizer-induced endosomal membrane destabilization.

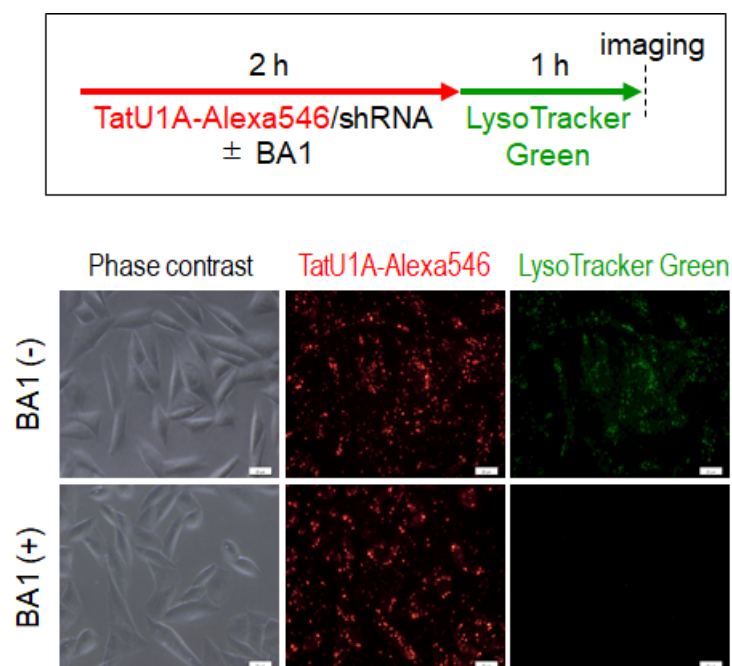


**Figure 2-3.** Acid vesicles disappeared in the presence of 200 nM BA1. Acid vesicles were stained with 2  $\mu$ M LysoTracker Green (Invitrogen) in T buffer for 1 h after the treatment (2 h) with BA1 and TatU1A-Alexa546/shRNA complex. Scale bars, 20  $\mu$ m.

Another effect of BA1 is the inhibition of endosomal trafficking (23). To exclude this effect, we treated the cells with BA1 after the endocytosis step (the condition iii). Even in the condition iii, BA1 interfered with the photoinduced endosomal escape (Fig. 2-2b). In addition, BA1 did not significantly inhibit endosomal accumulation of TatU1A-Alexa546/shRNA (Fig. 2-3 Alexa546 image, and Fig. 2-2 FAM image). These results suggest that photoinduced endosomal escape was suppressed by the effect of BA1 on endosomal acidification, and not on endosomal trafficking.

Next, endosomal pH was upregulated by the extracellular ammonium ion (10 mM  $\text{NH}_4\text{Cl}$ ), which quickly raises intralysosomal pH from  $\sim 4.8$  to  $\sim 6.2$  within 3 min in the previous report (36). We confirmed the disappearance of acidic vesicles stained by LysoTracker Green in the presence of 10 mM  $\text{NH}_4\text{Cl}$  (Fig. 2-5). As a result, PCI did not occur in the presence of 10 mM  $\text{NH}_4\text{Cl}$  (Fig. 2-4). These results, in addition to the experiments using BA1 (Fig. 2-2), indicate that acidification of endosomes prior to photoirradiation is important for causing PCI.

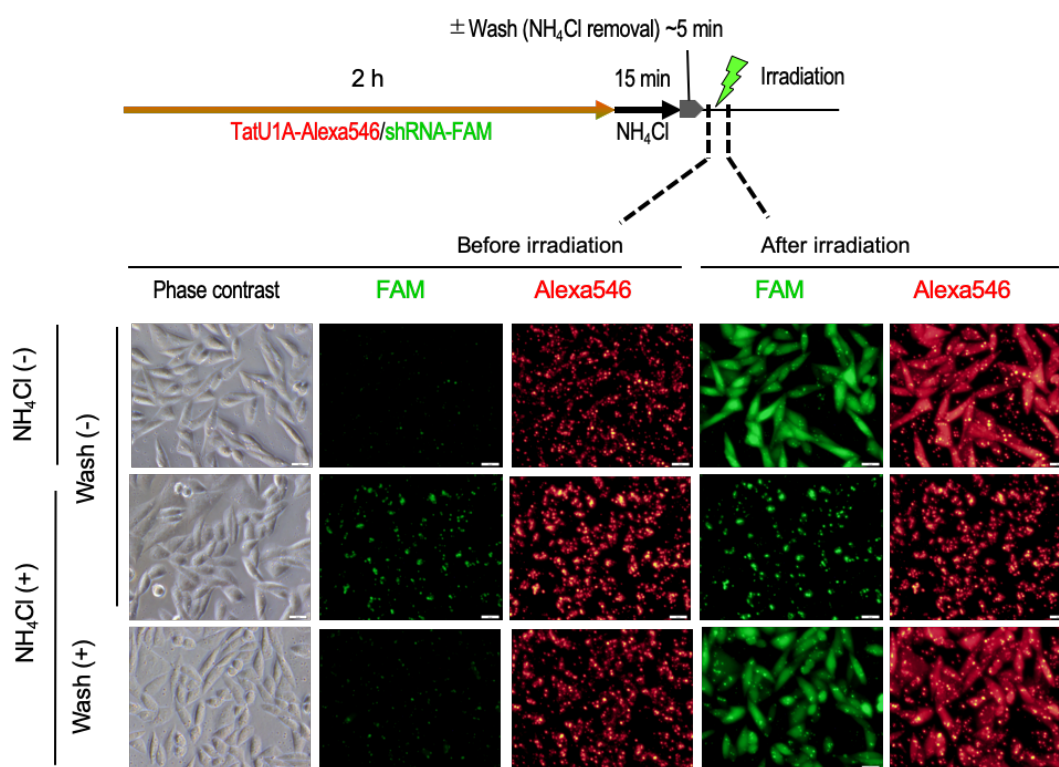


**Figure 2-4.** Influence of  $\text{NH}_4\text{Cl}$  in the medium on photoinduced cytosolic delivery of FAM-labeled RNA. After 2 h incubation with TatU1A-Alexa546/shRNA-FAM, cells were incubated with 10 mM  $\text{NH}_4\text{Cl}$  for 15 min

and irradiated. For the rescue experiment, cells were washed once with T buffer and incubated with T buffer for 5 min before irradiation. Scale bars, 20  $\mu\text{m}$ .

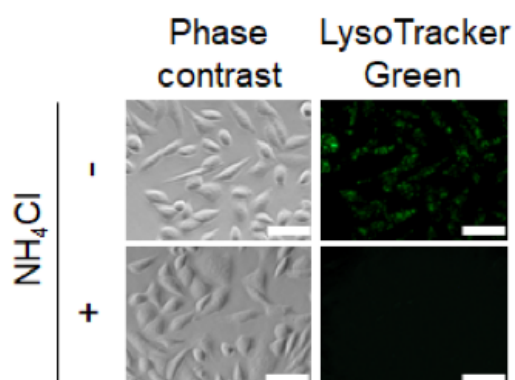


**Figure 2-5.** Acid vesicles disappeared in the presence of 10 mM  $\text{NH}_4\text{Cl}$ . Scale bars, 50  $\mu\text{m}$ .

Räägel et al. reported that endosomes that become leaky upon treatment with a TP10-fused protein and photo-induction, exhibit near-neutral, not acidic intravesicular pH (37). This seems to contradict with our results, which showed that photoinduced endosomal escape was suppressed by inhibiting endosomal acidification with BA1 or  $\text{NH}_4\text{Cl}$ . If near-neutral intravesicular pH is an important cause of endosomal leakage, inhibition of endosomal acidification would have enhanced photoinduced endosomal escape. However, these results are not necessarily contradictory, if near-neutral intravesicular pH is a result, not a cause of leaky endosomes. In our

experiments, photoinduced endosomal escape of TatU1A-Alexa546/shRNA was accompanied by an intravesicular pH increase (15).

### **Correlation between PCI and $[Ca^{2+}]_i$ increase**

Previous reports showed that photosensitization of cells accompanied  $[Ca^{2+}]_i$  increase (25). We investigated the relationship between PCI and  $[Ca^{2+}]_i$  increase using the TatU1A-PS/shRNA complex. The photoinduced  $[Ca^{2+}]_i$  increase was also confirmed in our system using the calcium indicator Fluo-4 AM (Fig. 2-6 and Fig. 2-7, left images).

We investigated whether the  $[Ca^{2+}]_i$  increase is related to the PCI-mediated endosomal escape. We imaged  $Ca^{2+}$  ions after irradiating the cells treated with TatU1A-PS/shRNA at 4 °C, which is known to inhibit endocytosis (38). TatU1A endocytosis was inhibited at 4 °C, as shown by the lack of TatU1A-Alexa633 colocalization with LysoTracker Green at 4 °C (Fig. 2-8). Endocytosis inhibition at 4 °C resulted in inhibition of cytosolic dispersion of TatU1A-PS/shRNA complexes (Fig. 2-6 and Fig. 2-7 right, Alexa images). The 4 °C treatment itself did not significantly affect  $[Ca^{2+}]_i$ , but the 4 °C treatment followed by photoirradiation induced  $[Ca^{2+}]_i$  increase, despite the lack of PCI (Fig. 2-6 and Fig. 2-7 right, Fluo-4 images). These

results suggest that the photoinduced  $[Ca^{2+}]_i$  increase is not dependent on the endosomal escape of the TatU1A-PS/shRNA complex.

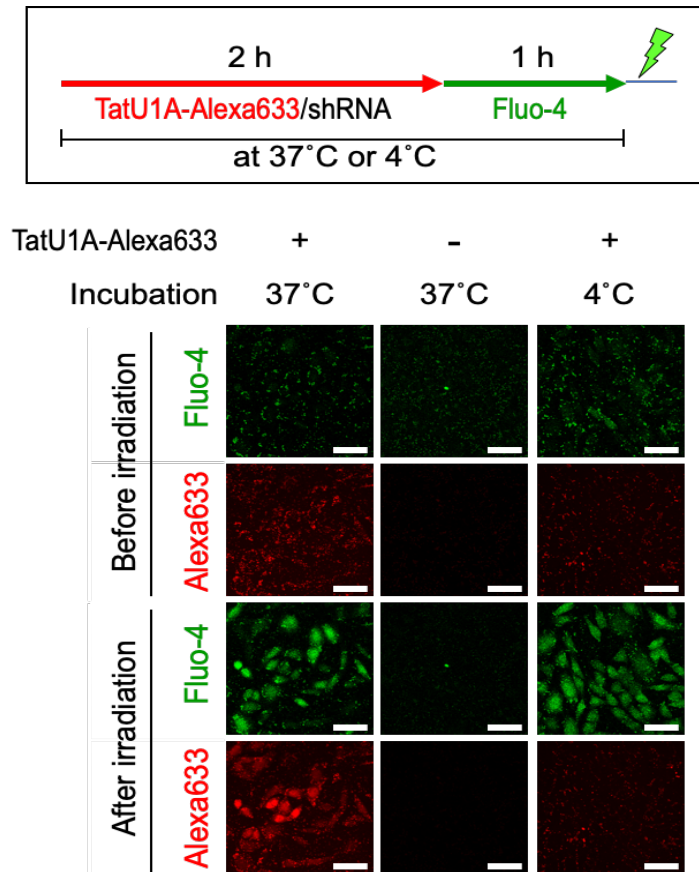


**Figure 2-6.** Correlation of  $Ca^{2+}$  signal intensity with endosomal escape of the CPP-cargo-photosensitizer (TatU1A-Alexa633) at 37 °C and 4 °C. Scale bars, 50 μm.

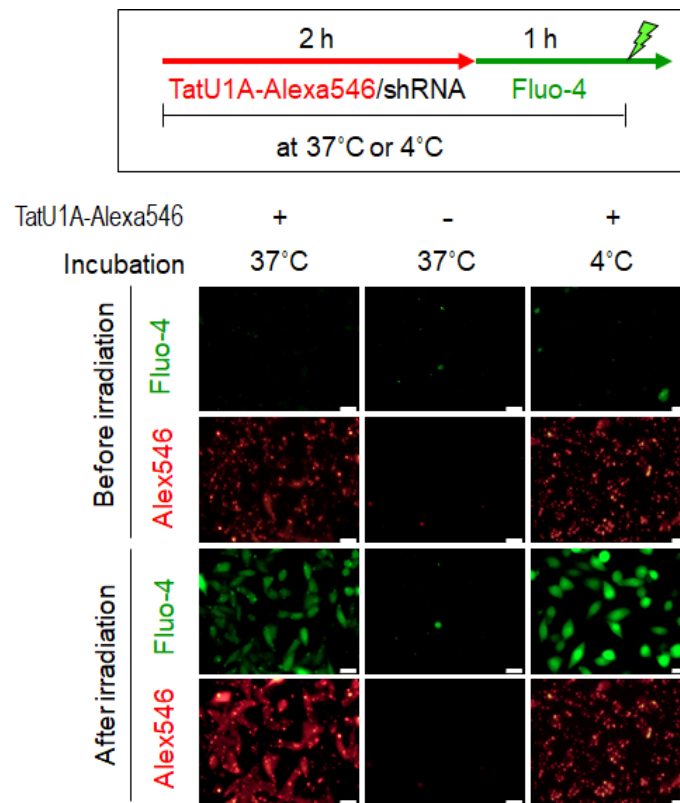


**Figure 2-7.** Correlation of  $\text{Ca}^{2+}$  signal intensity with endosomal escape of the CPP-cargo-photosensitizer (TatU1A-Alexa546) at 37 °C and 4 °C. Scale bars, 20  $\mu\text{m}$

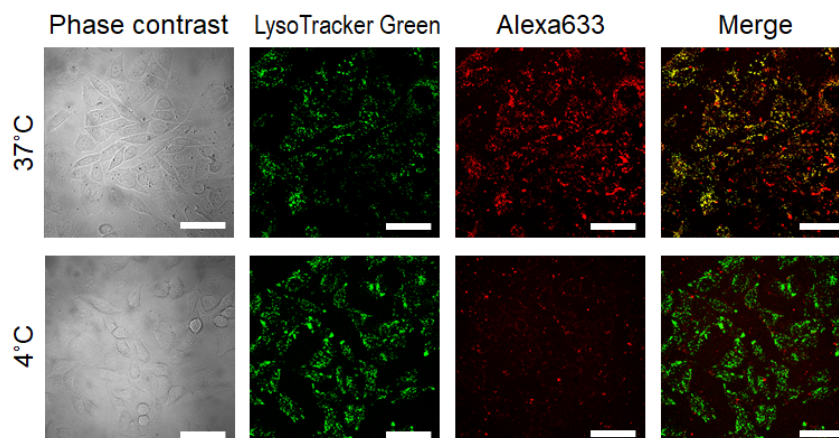


**Figure 2-8.** Localization of TatU1A-Alexa633 at 37 °C or 4 °C before photostimulation compared to LysoTracker Green. Scale bars, 50  $\mu\text{m}$

To further investigate correlation of PCI and the  $[Ca^{2+}]_i$  increase, cytosolic Alexa signal intensity was plotted against Fluo-4 signal intensity in individual cells treated with TatU1A-PS/shRNA and photoirradiated. Figure 2-9 shows that the endosomal release of TatU1A-PS/shRNA did not correlate with  $[Ca^{2+}]_i$  increase. The data scatter seen in Figure 2-9 is large; considerably high Alexa intensity was observed in some cells with low  $[Ca^{2+}]_i$  intensity, whereas low Alexa intensity was observed in other cells with high  $[Ca^{2+}]_i$  intensity. These results indicated that photoinduced cytosolic dispersion of TatU1A-PS/shRNA is independent of the  $[Ca^{2+}]_i$  intensity inside the cells. This suggests that  $[Ca^{2+}]_i$  increase does not relate to PCI. Although only a small fraction of the increased  $[Ca^{2+}]_i$  may relate to PCI, the results in Figures 2-6, 2-7 and 2-9 suggest that most of the increased  $[Ca^{2+}]_i$  is neither the cause nor the result of TatU1A-PS-mediated PCI.

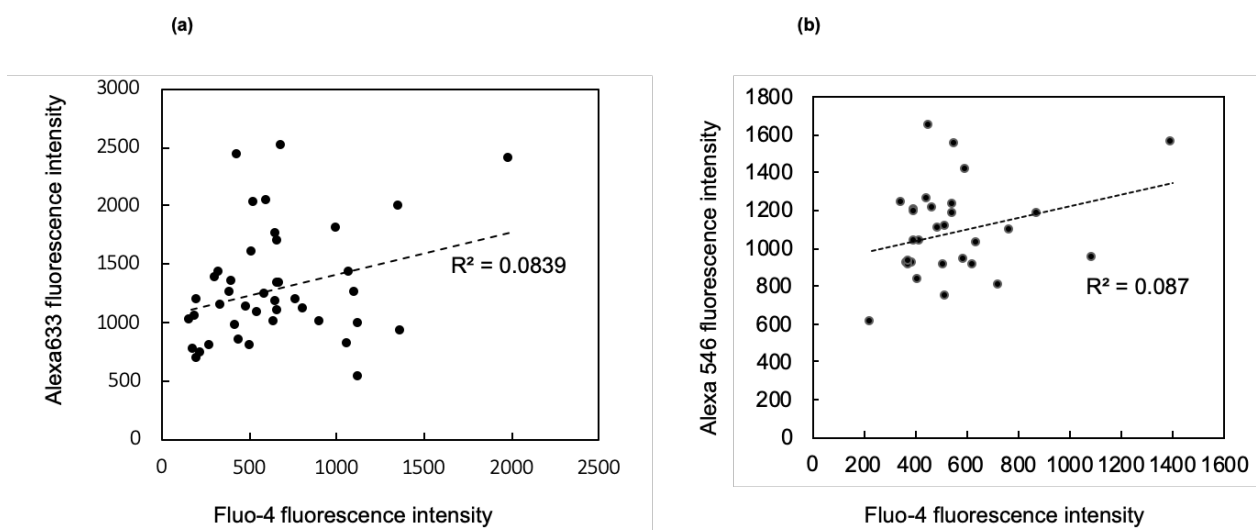


**Figure 2-9.** Scatter plots between cytoplasmic Alexa signal and Fluo-4 signal after photoinduced endosomal escape of TatU1A-Alexa633/shRNA (a) and TatU1A-Alexa546/shRNA (b) complexes at 37 °C.

### **The increased $[Ca^{2+}]_i$ mainly comes from extracellular sources**

Although the  $[Ca^{2+}]_i$  increase is almost irrelevant to PCI-induced endosomal escape in our system, light and TatU1A-PS still cause the  $[Ca^{2+}]_i$  increase (Fig. 2-6, 2-7). We investigated the origin of the  $Ca^{2+}$  ions resulting from TatU1A-PS and light treatment. We began by testing the influence of the extracellular calcium environment. After a 2 h treatment with TatU1A-Alexa546/shRNA followed by 1 h staining with Fluo-4, the extracellular calcium environment changed as described in the Figure 2-10 legend. Fluo-4 signal was detected in the 1.3 mM calcium environment, but the photoinduced increase of Fluo-4 signal was not observed in a calcium-free environment (Fig. 2-10). These results suggested that the  $[Ca^{2+}]_i$  increase depends on the extracellular calcium. Although the source of the increased  $[Ca^{2+}]_i$  is still debatable ( $Ca^{2+}$  influx or internal  $Ca^{2+}$  stores), the main source seems to be a  $Ca^{2+}$  influx in the TatU1A-PS system. Others reported that cell membrane  $Ca^{2+}$  channels might be involved in photoinduced  $Ca^{2+}$  influx (39). To confirm the contribution of  $Ca^{2+}$  channels, the voltage-sensitive  $Ca^{2+}$

channel were blocked using diltiazem before and after irradiation. As a result, the photoinduced influx of  $\text{Ca}^{2+}$  was decreased in the presence of diltiazem (Fig. 2-11). Thus, some fraction of the photoinduced  $\text{Ca}^{2+}$  influx is probably due to photodamage of plasma membrane  $\text{Ca}^{2+}$  channels.  $\text{Ca}^{2+}$  channel photodamage might be due to TatU1A-PS attached to the cell membrane while endosomal TatU1A-PS induces photochemical endosomal escape.

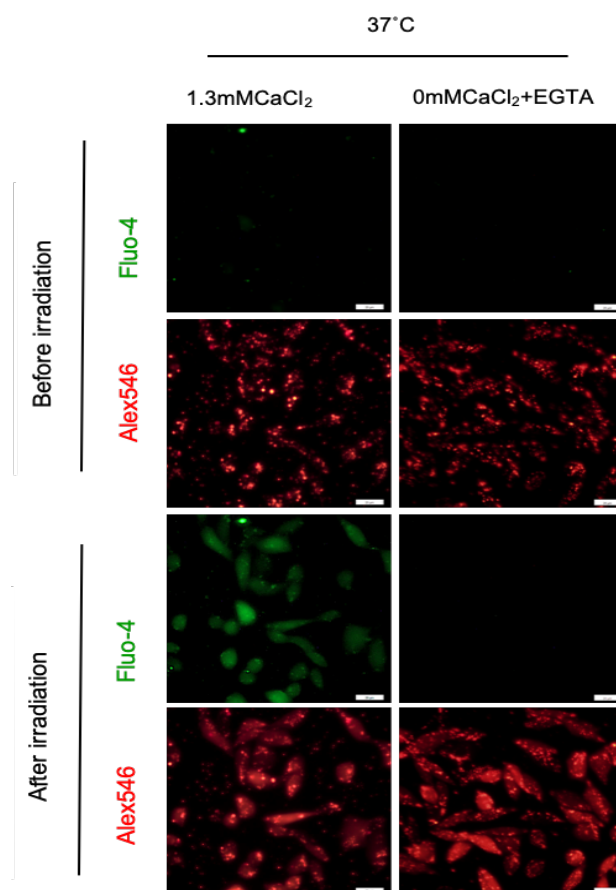


**Figure 2-10.** Cytosolic  $\text{Ca}^{2+}$  increase during PCI depend on extracellular calcium on at 37°C or 4°C. After a 2 h treatment with TatU1A-

Alexa546/shRNA followed by 1 h staining with Fluo-4, the cells were washed with T buffer (+CaCl<sub>2</sub>) or T buffer (-CaCl<sub>2</sub>) and irradiated in the respective buffer. T buffer (+CaCl<sub>2</sub>) included 1.3 mM CaCl<sub>2</sub> and 50 μM Fluo-4 AM. T buffer (-CaCl<sub>2</sub>) included no CaCl<sub>2</sub>, 0.2 mM EGTA and 50 μM Fluo-4 AM. Scale bars, 20 μm.

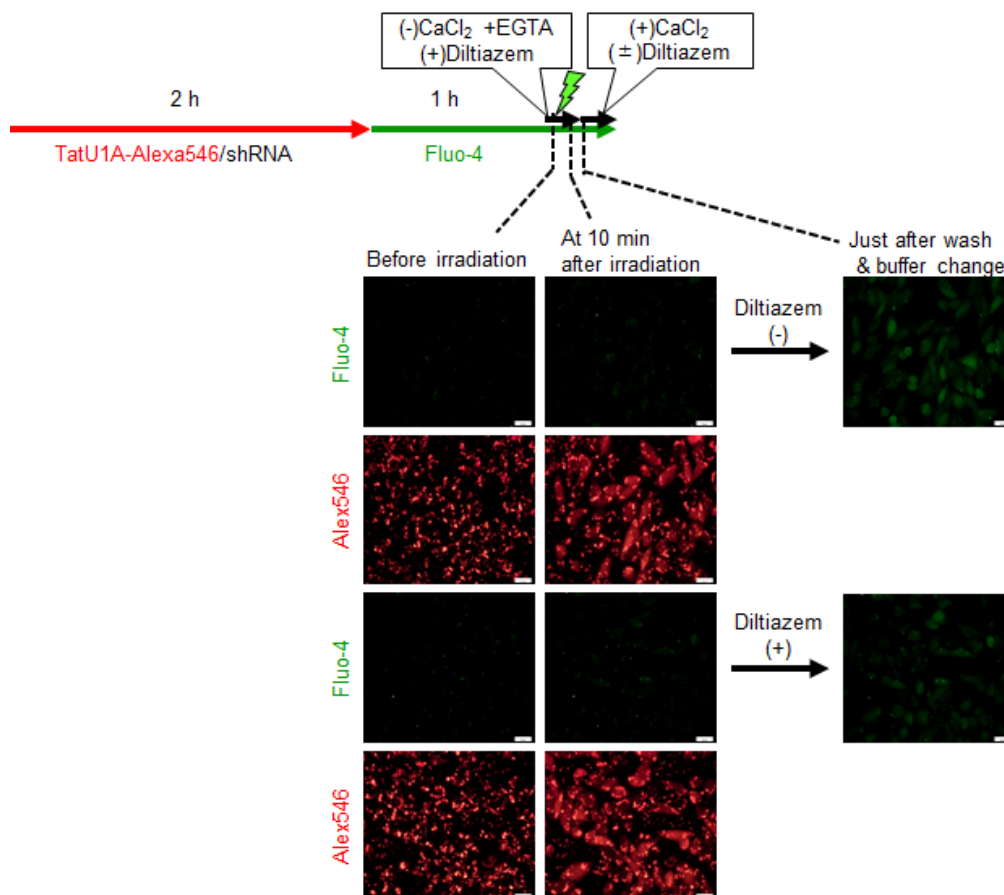


**Figure 2-11.** Photoinduced Ca<sup>2+</sup> influx blocked by diltiazem. CHO cells were treated with TatU1A-Alex546/shRNA and stained with Fluo-4. A Ca<sup>2+</sup> channel blocker, diltiazem was used as follows: after Fluo-4 staining, the cell

supernatant was replaced with T buffer (without CaCl<sub>2</sub>) including 0.2 mM EGTA and 10  $\mu$ M diltiazem. The cells were light irradiated as indicated in materials and methods. Ten min after irradiation, the cells were washed again with T buffer with or without 10  $\mu$ M diltiazem. Subsequently, images were quickly obtained by the fluorescence microscope. Scale bars, 20  $\mu$ m

## Conclusion

Here, we studied the role of heat, pH and calcium concentration on PCI-mediated endosomal escape of the CPP-cargo-photosensitizer conjugate TatU1A-PS/shRNA. The insignificant contribution of heat is confirmed by our result that the temperature during irradiation did not significantly affect photoinduced endosomal escape efficiency of the conjugate. The photoinduced endosomal escape was inhibited by a V-ATPase proton pump inhibitor. This indicates that the active proton pump is necessary for PCI and that PCI-mediated endosomal escape requires endosome acidification prior to photoirradiation. In addition, endosomal pH increase from  $\text{NH}_4\text{Cl}$  treatment prevented PCI, confirming the importance of the endosomal acidification before photostimulation. Photoinduced  $[\text{Ca}^{2+}]_i$  increase was observed at both 4 °C and 37 °C conditions with TatU1A-Alexa546/shRNA, indicating that the  $[\text{Ca}^{2+}]_i$  increase is not dependent on endocytosis. Moreover, cytoplasmic Alexa and  $\text{Ca}^{2+}$  intensities in individual cells after irradiation were not significantly correlated. These results suggest that the  $[\text{Ca}^{2+}]_i$  increase and PCI-mediated endosomal escape are independent phenomena in our TatU1A-PS system. Despite that, these phenomena are photoinduced at the same time. Overall, the findings in our study elucidate the suitable extra- and intracellular milieu conditions that are required for the

successful PCI occurrence. Our results might be useful for other PCI studies, in which a porphyrin/chlorin photosensitizer and cargo are administered separately. However, this needs to be confirmed by further studies. The PCI mechanism may partially differ depending on the cargo-delivery system and characteristics of the photosensitizer, such as its  $^1\text{O}_2$  quantum yield and the intracellular localization. In addition, this study implies the possibility of reducing side effects from PCI due to  $\text{Ca}^{2+}$  influx, since it seems to be independent of PCI in our TatU1A-PS system. Since our study suggested that photoinduced  $[\text{Ca}^{2+}]_i$  increase depends on extracellular calcium, unexpected  $\text{Ca}^{2+}$  influx, which may cause cellular damage, seems to be minimized by optimizing the culture conditions, without reducing the PCI efficiency.

## **Materials and Methods**

### **Preparation of TatU1A-Alexa**

The RNA carrier protein TatU1A, which has a C-terminal Cys residue, was prepared as previously described. Alexa Fluor 546 or 633 maleimide (Life Technologies, Carlsbad, CA) was attached to the C-terminus of TatU1A protein as follows: The purified TatU1A protein and Alexa Fluor 546 or 633 maleimide were mixed in a buffer containing 50 mM HEPES-KOH (pH 7.5), 100 mM  $(\text{NH}_4)_2\text{SO}_4$ , 150 mM imidazole, and 20% glycerol, and incubated at 25 °C for 1 h. The resulting TatU1A-Alexa546 or 633 was purified in a Centri-Sep spin column (Princeton Separations, Freehold Township, NJ) equilibrated with T buffer (20 mM HEPES-KOH (pH 7.4), 115 mM NaCl, 5.4 mM KCl, 1.8 mM  $\text{CaCl}_2$ , 0.8 mM  $\text{MgCl}_2$ , and 13.8 mM glucose). The protein concentration was determined using a Protein Assay Kit (Bio-Rad, Berkeley, CA). Labeling efficiencies of the carrier proteins were calculated by measuring the absorbance of the respective dyes. In all experiments, labeling efficiencies were adjusted to 20% using separately prepared unlabeled carrier proteins.

### **Short hairpin RNA (shRNA) preparation**

A FAM-labeled shRNA was purchased from JBioS (Saitama, Japan). The shRNA sequence used was 5'- GAU UAU GUC CGG UUA UGU ACA

UUG CAC UCC GUA CAU AAC CGG ACA UAA UCdT dT -3', with the U1A binding sequence is underlined. This is a non-specific shRNA in normal mammalian cells, but it contains an anti-luciferase sequence. A fluorescent dye (FAM) was attached at the 3' -end of the shRNA. The shRNA was annealed using incubation at 85 °C for 1 min to remove secondary structure and slow annealing (-1 °C/s) down to 4 °C. An shRNA used in Ca<sup>2+</sup> imaging is an unlabeled and non-specific shRNA with the anti-EGFP sequence 5'- GGC UAU GUC UAG GAG UGC ACA UUG CAC UCC GUG CGC UCC UGG ACG UAG CCU U -3', with the U1A binding sequence underlined. This shRNA was prepared by in vitro transcription as described (11).

### **Cell treatment with TatU1A-PS/shRNA complexes and photostimulation**

Chinese hamster ovary (CHO) cells were cultured in Ham's F-12 medium (Nacalai Tesque, Kyoto, Japan) supplemented with 10% fetal bovine serum (FBS) (Nichirei Biosciences, Tokyo, Japan), 100 units/mL penicillin, and 100 µg/mL streptomycin (Gibco, Invitrogen, Carlsbad, CA). To treat the cells with TatU1A-PS/RNA complex, TatU1A-PS (2 µM) and the FAM-labeled shRNA (200 nM) were mixed in T buffer and incubated at 37 °C for 10 min. CHO cells were grown on a 96-well plate to 70–80% confluence and treated for 2 h with the TatU1A-PS/RNA complex. After washing, the cells were visualized

using a fluorescence microscope (IX51, Olympus, Japan). For endosomal escape of the TatU1A-Alexa546/RNA complex, cells were irradiated with a 100 W mercury lamp (Olympus U-LH100HG) passed through the MWIG mirror unit (530-550 nm), a 40× objective lens, and a 12% ND filter. The light dose to the cells was 10 J/cm<sup>2</sup>. Unless otherwise stated, the light irradiation conditions for TatU1A-Alexa546/RNA complex are the same in all experiments in this study. The photoinduced endosomal escape efficiencies of the FAM-labeled RNA with each TatU1A-PS were calculated by counting the number of cells in which FAM fluorescence was dispersed within the cytosol after photostimulation (NF) and the total cell number (NT) using FAM fluorescence and phase-contrast images from the same area. The endosomal escape efficiency was defined as  $NF / NT \times 100 (\%)$ .

### **Photo-dependent endosomal escape of the RNA under various temperatures**

Cells were treated with the TatU1A-Alexa546/shRNA complex, irradiated, and visualized as described above. Just before photoirradiation, the cell temperature was regulated (30, 20 or 10 °C) as follows. For 30 °C, after exchanging the cell supernatant with the 37 °C medium, photoirradiation was started when the medium reached 30 °C based on the Type K thermocouple data

logger RX-450K (AS ONE, Japan). The 37 °C medium in the 96-well plate soon reached 30 °C in the room at 25±1 °C. For 20 °C, after exchanging the cell supernatant with the 4 °C medium, irradiation was started when the medium reached 20 °C. For 10 °C, after exchanging the cell supernatant with the 4 °C medium in a 96-well plate placed on 4 °C block incubator, the plate was quickly moved onto the fluorescence microscope and irradiation was started when the medium reached 10 °C.

### **Influence of a proton pump inhibitor on photo-dependent endosomal escape of the TatU1A-Alexa546/shRNA complex**

The cells were treated with TatU1A-Alexa546/shRNA complex, irradiated, and visualized as described above. The BA1 experiment was performed as follows. The cells were treated with 200 nM BA1 (AdipoGen Life Sciences, Switzerland) dissolved in T buffer at the following time points; (i) before treatment with the complex (1 h) (ii) at the same time as treatment with the complex (2 h), or (iii) after treatment with the complex (1 h).

### **Influence of NH<sub>4</sub><sup>+</sup>-induced increase of endosomal pH on photoinduced endosomal escape**

The cells were treated with the TatU1A-Alexa546/shRNA complex for

2 h as described above. The cell supernatant was replaced with T buffer with 10 mM NH<sub>4</sub>Cl. After a 15 min incubation at 37 °C in the buffer with 10 mM NH<sub>4</sub>Cl, the cells in the NH<sub>4</sub>Cl environment were irradiated and visualized as described above. To remove NH<sub>4</sub>Cl, cells were washed once and incubated with T buffer for 5 min. Irradiation was performed in the NH<sub>4</sub>Cl-free environment.

### **Ca<sup>2+</sup> imaging**

The cells were treated with TatU1A-Alexa546 or Alexa633/shRNA complex as described above, except for the incubation temperature (37 °C or 4 °C). The cells were stained with 50 μM Fluo-4 AM (Dojindo, Japan) in T buffer for 1 h. The staining was performed at the same temperature (37 °C or 4 °C) as TatU1A-Alexa546 or Alexa633/shRNA treatment. Cellular images were obtained using a confocal laser scanning microscope (FLUOVIEW FV1000, Olympus, Japan) or an epifluorescence microscope (IX51, Olympus, Japan). Fluorescence images were obtained through 60× objectives lens with the following settings: Alexa633 ( $\lambda_{\text{ex}} = 633 \text{ nm}$ ,  $\lambda_{\text{em}} = 650\text{-}750 \text{ nm}$ ), Alexa546 ( $\lambda_{\text{ex}} = 543 \text{ nm}$ ,  $\lambda_{\text{em}} = 555\text{-}655 \text{ nm}$ ) and Fluo4 ( $\lambda_{\text{ex}} = 488 \text{ nm}$ ,  $\lambda_{\text{em}} = 500\text{-}530 \text{ nm}$ ). Escape of the complex from the endosomes was induced by laser scanning (70% intensity) at 633 nm for TatU1A-Alexa633 or 543 nm for TatU1A-Alexa546. Cytosolic Alexa and Fluo-4 signal intensities in individual cells were analyzed with Olympus Fluoview software (FV10-ASW.4.2 version).

## References

1. Berg, K., P. K. Selbo, L. Prasmickaite, T. E. Tjelle, K. Sandvig, J. Moan, G. Gaudernack, Ø. Fodstad, S. Kjølslrud, H. Anholt, G. H. Rodal, S. K. Rodal, and A. Høgset (1999) Photochemical internalization: A novel technology for delivery of macromolecules into cytosol. *Cancer Res.* 59, 1180–1183.
2. Selbo, P. K., A. Weyergang, A. Høgset, O. J. Norum, M. B. Berstad, M. Vikdal, and K. Berg (2010) Photochemical internalization provides time- and space-controlled endolysosomal escape of therapeutic molecules. *J. Control. Release.* 148, 2-12.
3. Haug, M., G. Brede, M. Håkerud, A. G. Nedberg, O. A. Gederaas, T. H. Flo, V. T. Edwards, P. K. Selbo, A. Høgset, and Ø. Halaas (2018) Photochemical internalization of peptide antigens provides a novel strategy to realize therapeutic cancer vaccination. *Front. Immunol.* 9, 650.
4. Selbo, P. K., G. Sivam, Y. Fodstad, K. Sandvig, and K. Berg (2001) In vivo documentation of photochemical internalization, a novel approach to site specific cancer therapy. *Int. J. Cancer.* 92, 761–766.

5. Wang, J. T. W., F. Giuntini, I. M. Eggleston, S. G. Bown, and A. J. MacRobert (2012) Photochemical internalisation of a macromolecular protein toxin using a cell penetrating peptide-photosensitiser conjugate. *J. Control. Release.* 157, 305–313.
6. Sellevold, S., Q. Peng, A. S. V. Fremstedal, and K. Berg (2017) Photochemical internalization (PCI) of bleomycin is equally effective in two dissimilar leiomyosarcoma xenografts in athymic mice. *Photodiagn. Photodyn. Ther.* 20, 95–106
7. Oliveira, S., A. Hogset, and G. Storm (2008) Delivery of siRNA to the target cell cytoplasm: photochemical internalization facilitates endosomal escape and improves silencing efficiency, in vitro and in vivo. *Curr. Pharm. Des.* 14, 3686–3697.
8. Endoh, T., M. Sisido, and T. Ohtsuki (2009) Spatial regulation of specific gene expression through photoactivation of RNAi. *J. Control. Release.* 137, 241–245.
9. Matsushita-Ishiodori, Y., R. Kuwabara, H. Sakakoshi, T. Endoh, and T. Ohtsuki (2011) Photosensitizing carrier proteins for photoinducible RNA interference. *Bioconjug. Chem.* 22, 2222–2226.

10. Endoh, T., M. Sisido, and T. Ohtsuki (2008) Cellular siRNA delivery mediated by a cell-permeant RNA-binding protein and photoinduced RNA interference. *Bioconjug. Chem.* 19,1017–1024.
11. Shiraga, K., T. H. Soe, S. Matsumoto, K. Watanabe, and T. Ohtsuki (2018) Red and near-infrared light-directed cytosolic delivery of two different RNAs using photosensitive RNA carriers. *Bioconjug. Chem.* 29, 3174–3179.
12. Dingjan, I., D. R. J. Verboogen, L. M. Paardekooper, N. H. Revelo, S. P. Sittig, L. J. Visser, G. F. Von Mollard, S. S. V. Henriët, C. G. Figdor, M. Ter Beest, and G. Van Den Bogaart (2016) Lipid peroxidation causes endosomal antigen release for cross-presentation. *Sci. Rep.* 6, 22064.
13. Girotti, A. W (1998) Lipid hydroperoxide generation, turnover, and effector action in biological systems. *J. lipid. Res.* 39, 1529–42.
14. Wang, T. Y., M. D. J. Libardo, A. M. Angeles-Boza, and J. P. Pellois (2017) Membrane oxidation in cell delivery and cell killing applications. *ACS Chem. Biol.* 12, 1170-1182.
15. Ohtsuki, T., S. Miki, S. Kobayashi, T. Haraguchi, E. Nakata, K. Hirakawa, K. Sumita, K. Watanabe, and S. Okazaki (2015) The molecular mechanism of photochemical internalization of cell

- penetrating peptide-cargo-photosensitizer conjugates. *Sci. Rep.* 5, 18577.
16. Mellman, I., R. Fuchs, and A. Helenius (1986) Acidification of the endocytic and exocytic pathways. *Annu. Rev. Biochem.* 55, 663–700.
  17. Hu, Y. B., E. B. Dammer, R. J. Ren, and G. Wang (2015) The endosomal-lysosomal system: from acidification and cargo sorting to neurodegeneration. *Transl. Neurodegener.* 4, 18.
  18. Gruenberg, J., and F. R. Maxfield (1995) Membrane transport in the endocytic pathway. *Curr. Opin. Cell Biol.* 7, 552–563.
  19. Odegard, A. L., M. H. Kwan, H. E. Walukiewicz, M. Banerjee, A. Schneemann, and J. E. Johnson (2009) Low endocytic pH and capsid protein autocleavage are critical components of flock house virus cell entry. *J. Virol.* 83, 8628–8637.
  20. Maxson, M. E., and S. Grinstein (2014) The vacuolar-type H<sup>+</sup>-ATPase at a glance - more than a proton pump. *J. Cell Sci.* 127, 4987–4993.
  21. Yoshimori, T., A. Yamamoto, Y. Moriyama, M. Futai, and Y. Tashiro (1991) Bafilomycin A1, a specific inhibitor of vacuolar-type H<sup>+</sup>-ATPase, inhibits acidification and protein degradation in lysosomes of cultured cells. *J. Biol. Chem.* 266, 17707–17712.

22. Bayer, N., D. Schober, E. Prchla, R. F. Murphy, D. Blaas, and R. Fuchs (1998) Effect of bafilomycin A1 and nocodazole on endocytic transport in HeLa cells: implications for viral uncoating and infection. *J. Virol.* 72, 9645-9655.
23. Wang, C., T. Zhao, Y. Li, G. Huang, MA. White, and J. Gao (2017) Investigation of endosome and lysosome biology by ultra pH-sensitive nanoprobe. *Adv. Drug Deliv. Rev.* 113, 87-96.
24. Görlach, A., K. Bertram, S. Hudecova, and O. Krizanova (2015) Calcium and ROS: A mutual interplay. *Redox Biol.* 6, 260-271.
25. Hoorelbeke, D., E. Decrock, V. Van Haver, M. De Bock, and L. Leybaert (2018) Calcium, a pivotal player in photodynamic therapy? *Biochim. Biophys. Acta.* 1865, 1805-1814.
26. Tarr, M., A. Frolov, and D. P. Valenzano (2001) Photosensitization-induced calcium overload in cardiac cells: direct link to membrane permeabilization and calcium influx. *Photochem. Photobiol.* 73, 418-424.
27. Hu, S. L., P. Du, R. Hu, F. Li, and H. Feng (2014) Imbalance of Ca<sup>2+</sup> and K<sup>+</sup> fluxes in C6 glioma cells after PDT measured with scanning ion-selective electrode technique. *Lasers Med. Sci.* 29, 1261–1267.

28. Wu, D. P., T. Y. Lin, L. R. Bai, J. L. Huang, Y. Zhou, N. Zhou, S. L. Zhong, S. Gao, and X. X. Yin (2017) Enhanced phototoxicity of photodynamic treatment by Cx26-composed GJIC via ROS-, calcium- and lipid peroxide-mediated pathways. *J. Biophotonics*. 10, 1586–1596.
29. Ding, X., Q. Xu, F. Liu, P. Zhou, Y. Gu, J. Zeng, J. An, W. Dai, and X. Li (2004) Hematoporphyrin monomethyl ether photodynamic damage on HeLa cells by means of reactive oxygen species production and cytosolic free calcium concentration elevation. *Cancer Lett*. 216, 43–54.
30. Gerasimenko, J. V., A. V. Tepikin, O. H. Petersen, and O. V. Gerasimenko (1998) Calcium uptake via endocytosis with rapid release from acidifying endosomes. *Curr. Biol*. 8, 1335–1338.
31. Christensen, K. A., J. T. Myers, and J. A. Swanson (2002) pH-dependent regulation of lysosomal calcium in macrophages. *J. Cell Sci*. 115, 599–607.
32. Muthukrishnan, N., G. A. Johnson, J. Lim, E. E. Simanek, and J. P. Pellois (2012) TAT-mediated photochemical internalization results in cell killing by causing the release of calcium into the cytosol of cells. *Biochim. Biophys. Acta*. 1820, 1734–1743.

33. Shim, G., S. Ko, D. Kim, Q. V. Le, G. T. Park, J. Lee, T. Kwon, H. G. Choi, Y. B. Kim, and Y. K. Oh (2017) Light-switchable systems for remotely controlled drug delivery. *J. Control. Release.* 267, 67–79.
34. Bowman, E. J., A. Siebers, and K. Altendorf (1988) Bafilomycins: a class of inhibitors of membrane ATPases from microorganisms, animal cells, and plant cells. *Proc. Natl. Acad. Sci. USA.* 85, 7972-7976.
35. Brabec, M., D. Schober, E. Wagner, N. Bayer, R. F. Murphy, D. Blaas, and R. Fuchs. (2004) Opening of size-selective pores in endosomes during human rhinovirus serotype 2 in vivo uncoating monitored by single-organelle flow analysis. *J. Virol.* 79, 1008–1016.
36. Ohkuma, S., and B. Poole (1978) Fluorescence probe measurement of the intralysosomal pH in living cells and the perturbation of pH by various agents. *Proc. Natl. Acad. Sci. USA.* 75, 3327–3331.
37. Räägel, H., M. Hein, A. Kriiska, P. Säälük, A. Florén, Ü. Langel, and M. Pooga (2013) Cell-penetrating peptide secures an efficient endosomal escape of an intact cargo upon a brief photo-induction. *Cell Mol Life Sci.* 70, 4825-39.
38. Schaeffer, S. F (1978) Membrane recycling in the cone cell endings of the turtle retina. *J. Cell. Biol.* 79, 802–825.

39. Joshi, P. G., K. Joshi, S. Mishra and N. B. Joshi (1994)  $\text{Ca}^{2+}$  influx induced by photodynamic action in human cerebral glioma (U-87 MG) cells: possible involvement of a calcium channel. *Photochem. Photobiol.* 60, 244-248.

## **Chapter 3**

### **Application of PCI as a Photo-Dependent RNA Delivery**

#### **Strategy to Mouse Embryo**

## **Abstract**

The cell fate decision to inner cell mass (ICM) and trophectoderm (TE) in blastocyst stage embryo starts from the early 8 to 16-cell stage due to the difference of cell polarity in outer and inner lying cells. Understanding the molecular mechanism of these cellular differentiation in embryogenesis will be a great help for further development of assisted reproduction techniques (ART) such as in vitro fertilization. Recently, the photoinduced cytosolic dispersion of RNA (PCDR) using TatU1A-photosensitizer conjugate in cultured cells has been established by our group. As PCDR method using photosensitive RNA carrier has an ability to control RNA function in temporal and spatial manner, introduction of RNAs to the individual cell by PCDR is a very useful approach for studying cell differentiation mechanism in early embryogenesis. In this study, PCDR was firstly confirmed in mouse embryos by using TatU1A-Alexa546/FAM shRNA. Photo-dependent knockdown of d1EGFP was demonstrated in 4-cell embryos, indicating that spatial regulation of gene expression in mouse embryo was achieved by PCDR method. Finally, anti-aPKC shRNA, related to Par6-aPKC polarization, was introduced into a single blastomere of four-cell embryos and down regulation of PKC in early embryos development

was briefly discussed. Our findings showed that PCDR is a promising approach for the study of the developmental process of early embryogenesis.

## **Introduction**

The first two cell lineages in preimplantation embryo: inner cell mass (ICM) and outer cell trophectoderm (TE) differentiation occurs at the fourth cleavage of embryos from 8 to 16 cell transition. Initialization of these two cells population is generally assumed by two models, inside-outside model that proposed the cell fate decision is dependent on the position of cells (1) and a polarity model that proposed ICM and TE differentiation is aligned by subcellular distribution of cell polarity due to asymmetric division of cells (2). A number of studies have agreed to both models (3) but there is still needed to understand molecular details of each proposed models. In fact, a series of transcriptional factors and polarity regulators control mouse embryo development (4).

During preimplantation, embryo development occurs as a serial event (Fig. 3-1). As a first cell cleavage, a fertilized egg divides into two daughter cells. While the cleavage is repeated up to 8-cell stage, all blastomeres (cells are known as blastomeres) are morphological identical, except embryos undergo compaction, which of each cell obtaining cell-cell

contact basolateral domain and contact-free surface domain. The contacting cell to each other is sufficient to the establishment of polarity but not necessary for the maintenance of polarity (5). After the cell polarity starts arising along with compaction to apical surface of 8-cells (known as early morula stage) (6) and passes from 8 to 16 cells transition due to asymmetric cell division, the first two cell lineages are formed at 16-cell embryos depending on polarity inheritance or absence (Fig. 3-1). But some embryos undergo symmetric cell division and both daughter cells inheriting polarity retain as the outside cells (7).

There are three subfamilies of PKC isoforms (serine/threonine kinases family) according to their difference in sensitivity to activators and co-factors such as negatively charged phospholipids, calcium and diacylglycerol (DAG). The conventional PKCs (cPKCs) are  $\alpha$ ,  $\beta$  I,  $\beta$  II, and  $\gamma$ , the novel PKCs (nPKCs) are  $\delta$ ,  $\theta$ ,  $\eta$ ,  $\epsilon$  and  $\mu$ , and atypical PKCs (aPKCs) are  $\lambda$  or  $\iota$  and  $\zeta$  (8,9). The partitioning defective (Par) and aPKC form a complex which largely regulate apical cell polarity during embryogenesis. Two Par molecules, Par6 and Par3, and aPKC are restricted to the contact-free surface of outer cells (10) and also regulate cell-cell contact localized proteins such as Par1/EMK, Scribble and Lg1 (5,11). The molecular mechanism that regulates cell fate-controlled genes expression is governed

by position- and polarity- dependent Hippo signaling (11). Thus, the establishment of Par6-aPKC polarization at the outer edge of the cells relates to Hippo signaling. For example, the Par6-aPKC defected embryos blocked Yap location to nucleus by activating Hippo signaling at 32-cell embryos (11). The proposed molecular mechanism is as follow (Fig. 3-1): at 32-cell stage embryos, while Par6-aPKC system is active, Hippo signaling becomes weak in the outer cells. Polarized Par6-aPKC sequester Amot to inactivate Lats protein kinase and nuclear translocation of Yap, which is a coactivator of Tead4, was occurred (12). Consequently, activated Tead4 triggers expression of Cdx2 in these cells (13). In the inner cells, Cdx2 is not expressed due to the phosphorylated Amot which leads to activation of Yap gene while Hippo signaling is active. Cdx2 is one of the prominent TE specific marker genes as like as Eomes and Gata3 (14,15). As mutual suppression is found between Cdx2 and either Oct 4 or Nanog in each other, expression of Oct 4 and Nanog are restricted to ICM while Cdx2 is off in that blastomere (16,17). Since it has been found that Cdx2 fails to express in polarized cells, some researchers suggested that the expression of TE-regular Cdx2 in outer cell is controlled by Par6-aPKC polarization (3,4).

Absence of certain transcription factors that regulate cell fate specification and cell polarity regulators that allocate cell in the correct

positions cause failure of implantation and eventually lead to embryonic lethality after implantation. For example, both of Eomes and Cdx2 homozygous mutant embryos die around the time of implantation (18). The aPKC  $\lambda$  depleted cells induced destabilization of cell polarity (19) and potentially lead to incorrect allocation of cells to inner cell mass (20). Inhibition of PKCs at 4 to 8 cell transition with cPKCs inhibitor, sphingosine and nPKCc inhibitor, calphostin C prevent compaction and polarization (21). The Par6B deficient embryos cause no blastocoel formation (22), and the aPKC deficient embryos die after implantation (23). Therefore, first cell differentiation in early embryo is a critical event that affects implantation of the embryo on mother's uterus and even survival of embryos after implantation.

We have developed the photoinduced chemical internalization of RNA (PCDR) method by using photosensitive RNA carrier (24). We have reported that PCDR approach can facilitate delivery of RNA to the cytosol with no significant cytotoxicity. The RNA carrier molecule is composed of a cell-penetrating peptide (CPP), an RNA-binding protein (RBP), and a photosensitizer (PS). As it was already mentioned in chapter1, a Tat CPP which is genetically fused with U1A from the RNA binding domain of U1 small nuclear ribonucleoprotein A and dyes, such as Alexa 546 or 633, as a

PS have been used to deliver small RNAs by light irradiation. Since we have reported that PCDR is an efficient approach to the spatial regulation of gene expression, e.g single cell RNAi (25), application of this technique to study of regional specific gene functions in early cell differentiation of mouse embryo will be a merit for further development of assisted reproduction techniques (ART). Although some findings of evidences have reported that there is an interplay between the Par-aPKC system and Cdx2, in cell lineage specification, but it is still controversial (11, 26, 27). Moreover, how these polarity and transcription regulators assigned cells to ICM and TE specification is also unclear. Therefore, in this study, we will evaluate role of Par6-aPKC polarization in the regulation of TE-specific marker, Cdx2 in embryogenesis by photo-dependent introduction of anti-aPKC shRNA (hereafter referred to as shaPKC), to an outside or inside single blastomere of embryos. Cell differentiation to TE or ICM will be tracked by fluorescent markers and embryos will be diagnosed by its shape and immunostaining of differentiation markers (Cdx2, Oct4, etc.)

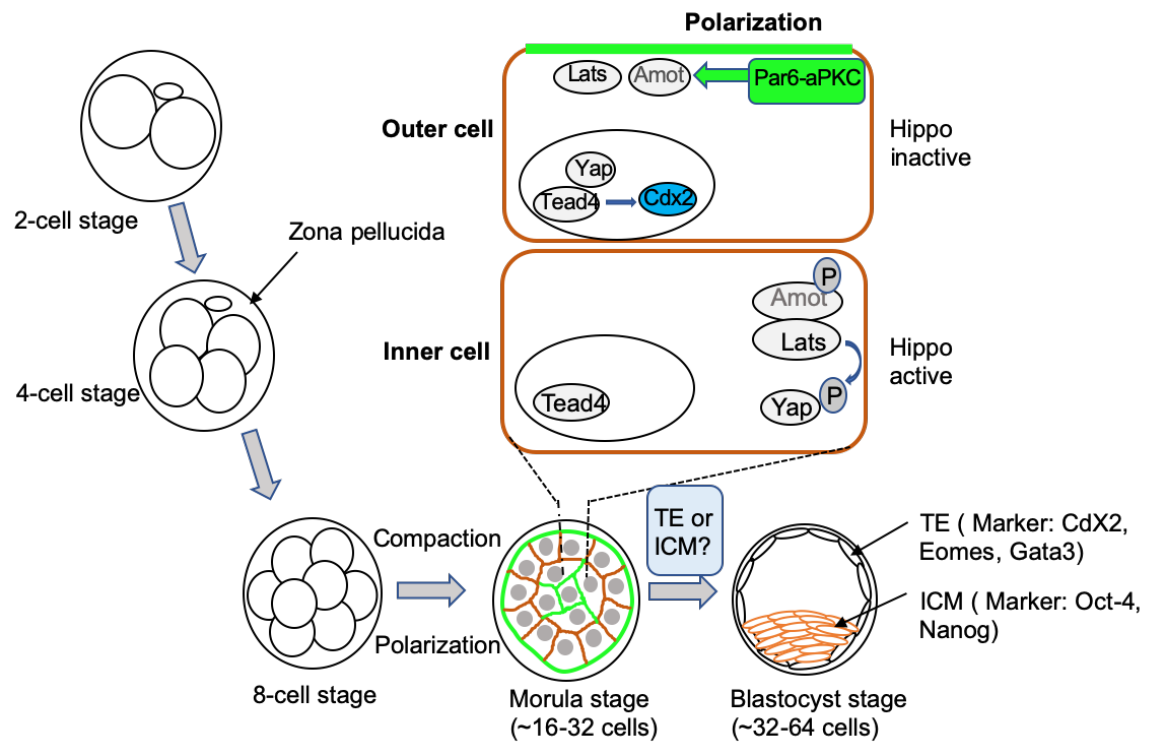


**Figure 3-1.** The role of Par6-aPKC polarization in early mouse embryogenesis

## **Results and Discussion**

### **Photoinduced RNA internalization by single cell of mouse embryo**

Previously, we have studied photoinduced delivery of shRNA by PCDR in culture cells. We have demonstrated that photo-dependent delivery of TatU1A-PS/ Fluorescein (FAM)-labeled RNA (shLuc-FAM) conjugate into CHO cells (28). After endosomal release of shLuc-FAM by light irradiation, the fluorescence intensity of FAM was increased in cytosol, where pH is around 7.2, a higher pH than inside endosome (24). The fluorescence increase of shLuc-FAM was due to pH difference between endosome and cytosol. To confirm this PCDR approach in mouse embryo, TatU1A-Alexa546 was used to deliver shLuc-FAM into 4-cell embryos by laser irradiation. Zona free 4-cell embryos were incubated in TatU1A-Alexa546/shLuc-FAM complex solution for 3h in order to enter the complex into the cells via endocytosis. After irradiation at a single cell by 546-nm laser of confocal microscopy, TatU1A-Alexa546 was released to the cytosol of an irradiated cell and FAM labelled shRNA was internalized by that irradiated single cell, showing dispersion of photosensitizer and FAM fluorescence in cytosol while others of 4-cell embryo were detected no apparent fluorescence of both (Fig. 3-2). Embryos were kept growing to

blastocyst stage (~32-46 cells), which is a late stage of preimplantation embryo. There were no significant disturbances in development of embryos to this stage after photostimulation. This result indicated that efficient delivery of a certain cargo molecule to a targeted cell could be achieved by light controlled manner and PCDR has a potency to regulate specific gene expression without intervening the progress in embryonic development.

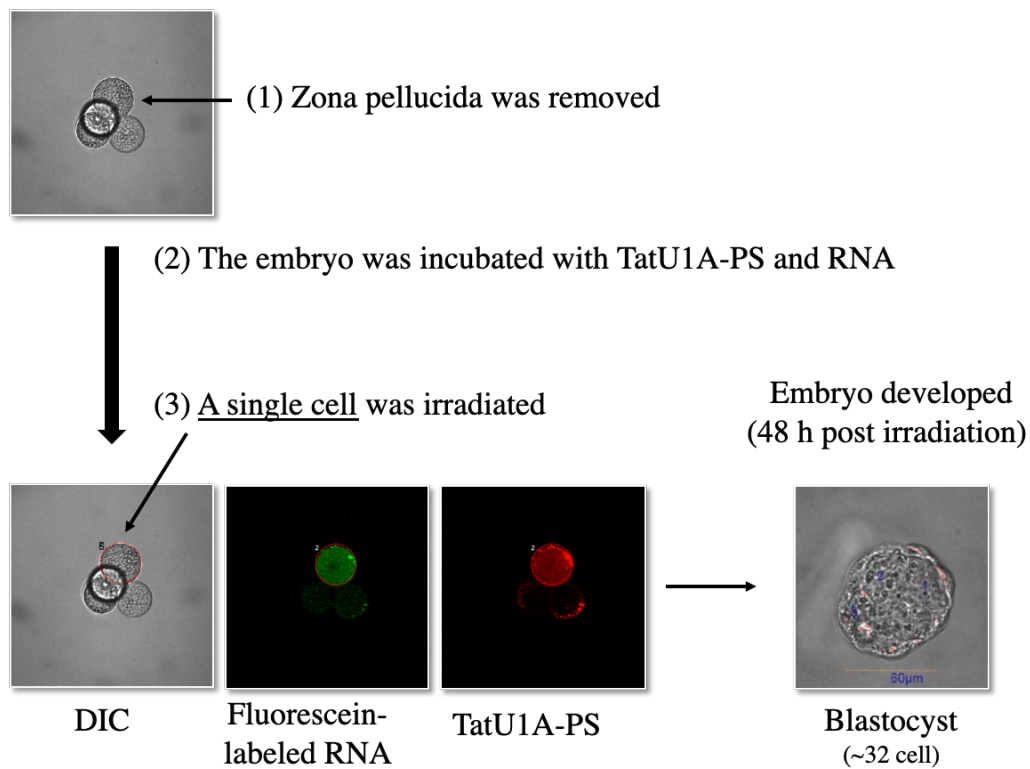


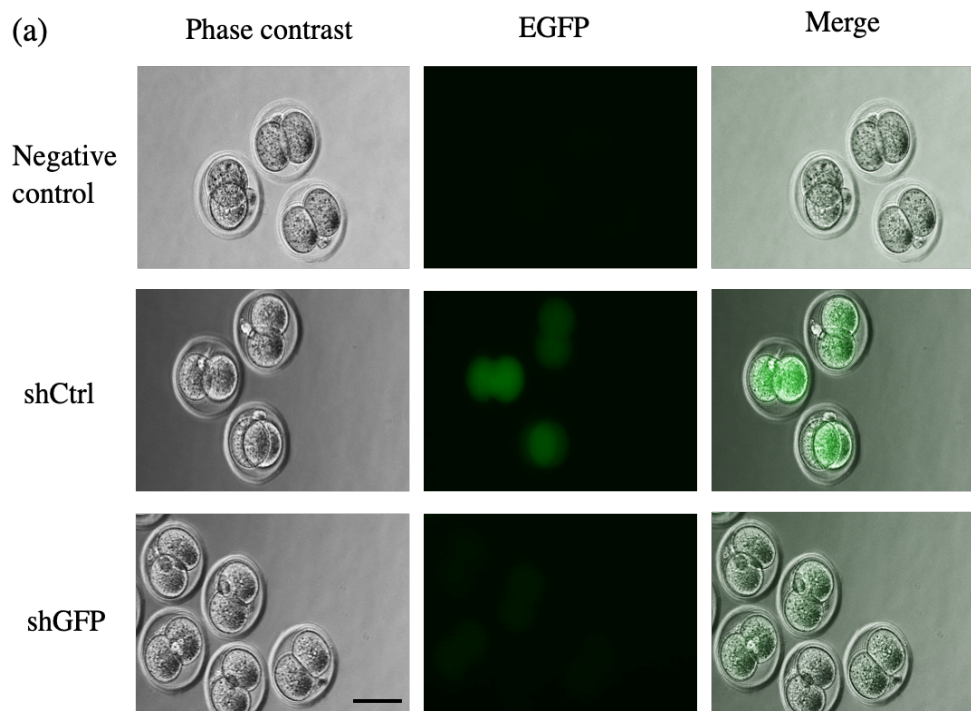
**Figure 3-2.** Photoinduced RNA internalization by a single cell of mouse embryos

## **Photo-dependent knockdown of EGFP in mouse embryo**

Next, in order to demonstrate photo-dependent regulation of specific gene expression, we aimed to silence enhanced green fluorescence protein (EGFP) expression in mouse embryos. Before performing photo-dependent knockdown of EGFP, first we confirmed EGFP silencing efficiency of anti-EGFP shRNA with U1A binding sequence (hereafter referred to as shGFP) to exogenously expressed destabilized EGFP (d1EGFP) in mouse embryos by microinjection. In this study, single cell embryos were used to coinject shGFP and *in vitro*-synthesized d1EGFP mRNA. To compare EGFP knockdown efficiencies, the non-targeted shRNA (shCtrl) with U1A binding sequence was injected together with d1EGFP mRNA. As a result, after 24h microinjection, the significant reduction of EGFP fluorescence was observed at two-cell stage shGFP microinjected embryos (Fig. 3-3a). The results indicated that exogenous EGFP mRNA expression was inhibited by microinjection of shGFP.

As our purpose is to establish photoinduced RNAi in mouse embryo, the similar EGFP knockdown experiment was performed by PCDR. In this study, BFP and d1EGFP mRNA were initially expressed in single cell of 4-cell embryo by microinjection. When both BFP and EGFP signals were clearly detected in the single cell, about 3h after microinjection, TatU1A-

Alexa546/shGFP or shCtrl treated embryos were irradiated by laser light at 546nm (Fig. 3-3b). As a result, specific silencing of EGFP was observed at 30h after light irradiation while BFP fluorescence signal was still detected in it (Fig. 3-3b). The laser irradiation neither cause cellular damages nor interfere the development of embryos. Thus, this result provided an evidence that regional specific regulation of gene expression via photoinduced RNAi in mouse embryo could be achieved by PCDR.



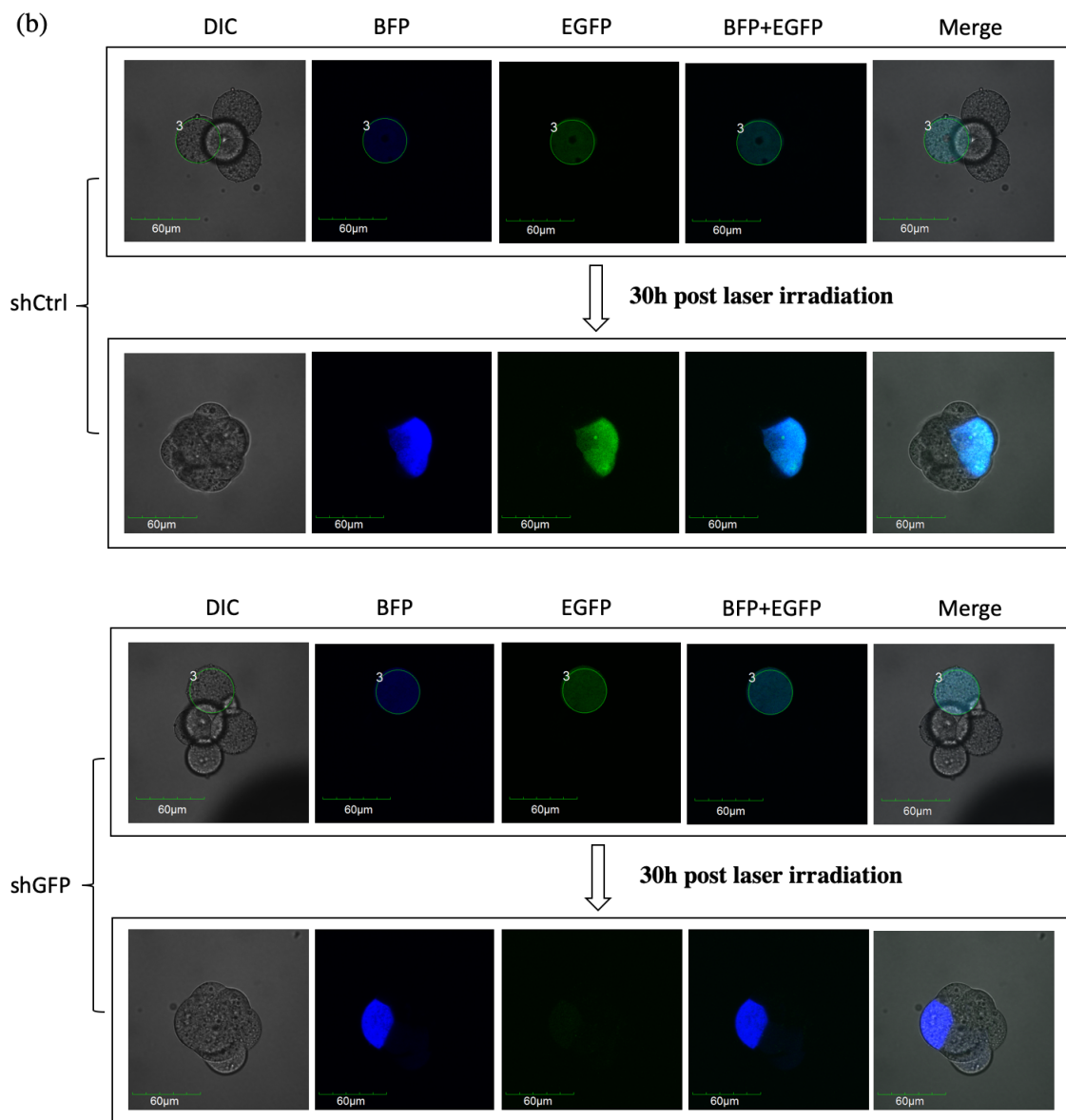


**Figure 3-3.** EGFP silencing in mouse embryos. (a) EGFP knockdown was performed by microinjection of shGFP. Coinjected shGFP or shCtrl with d1EGFP mRNA to single cell embryo. At 24h after microinjection, EGFP silencing was observed at 2-cell embryos. Scale bar represents 60 μm. (b) EGFP knockdown occurred through photoinduced RNAi by laser irradiation.

At 3h after microinjection of BFP and EGFP mRNA, a single cell expressing BFP and EGFP, indicated by a circle, was irradiated by a laser at 546nm. The EGFP silencing was observed at 30 h after the laser irradiation. Scale bars represent 60  $\mu$ m.

### **Reduction of aPKC expression at apical cortex of outside cells**

To study the role of Par6-aPKC polarization in TE and ICM cell differentiation mechanism in early mouse embryogenesis, we targeted to down-regulate aPKC  $\lambda$  in 4-cell stage. The studies of various PKC isotypes in preimplantation mouse embryo were previously discussed that the expression and localization of isoforms are different, and change associated with development of embryos (8,9). Among the isotypes, the aPKC  $\lambda$  is one of the highly expressed isotypes from unfertilized eggs (maternal) to blastocyst stage (9). Thus, we aimed to investigate whether interfering the expression of aPKC through RNAi at a single blastomere of the 4-cell embryo, at which apical polarization was not yet established, cause any abnormality in the outside progeny of the injected blastomere due to polarity defects. We used H2BmCherry mRNA as a cell tracer and co-injected together with shaPKC to a random single blastomere of 4-cell embryo. Since aPKC localized to the apical cortex of outer cells, its knockdown effect was

examined, (based on H2BmCherry expressed cells), at the outer cells of morula and blastocyst stage embryos (Fig. 3-4 and 3-5). The results showed that significant reduction of aPKC fluorescence at the apical region of outer cells in shaPKC injected embryos when compare to the apical cortex of outside cells in shCtrl injected embryos (Fig. 3-4a and Fig. 3-5c). The decrease of cell numbers in shaPKC injected embryos was observed at morula stage, indicating that even aPKC depletion in a blastomere can delay the development of embryo (Fig. 3-4b). The H2BmCherry expressed cells were assumed as progeny cells of shRNAs injected cells. When embryos were observed at blastocyst stage, progeny of shaPKC injected cells of embryos were also detected at outside position with a reduction of apical aPKC expression (Fig. 3-5b). It seems downregulation of aPKC in a single blastomere could not cause significant impact on the allocation of cells to TE. But there may need further confirmations, *i.e.* staining embryos with TE/ICM specific makers such as Cdx2 and Oct4, to reach a certain conclusion. In this study, the results of microinjection of shaPKC and H2BmCherry mRNA also showed that we can trace the injected cells with a significant aPKC knockdown efficiency. These results encourage us to apply a similar experimental condition for the study of photo-dependent aPKC regulation by PCDR method in future.

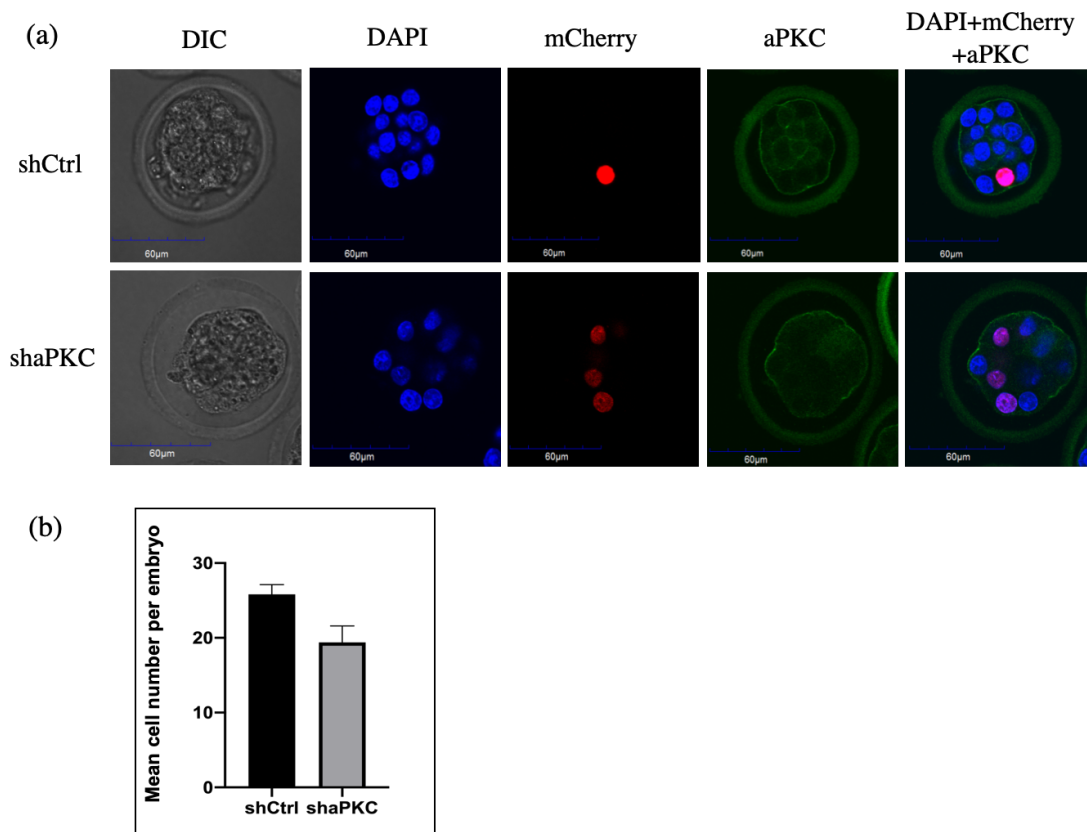


**Figure 3-4.** Effects of aPKC knockdown on late morula stage embryos. (a) Reduction of aPKC expression at the apical region of outer cells in shaPKC injected embryos. The H2BmCherry mRNA (red) was co-injected with shaPKC or shCtrl. Embryos were immunostained with aPKC  $\lambda$  (Green) antibody and the nuclei were stained with DAPI (green). (b) Reduction of cell numbers in shaPKC injected embryos. Error bars represent standard deviation of the mean value (n=5 each).

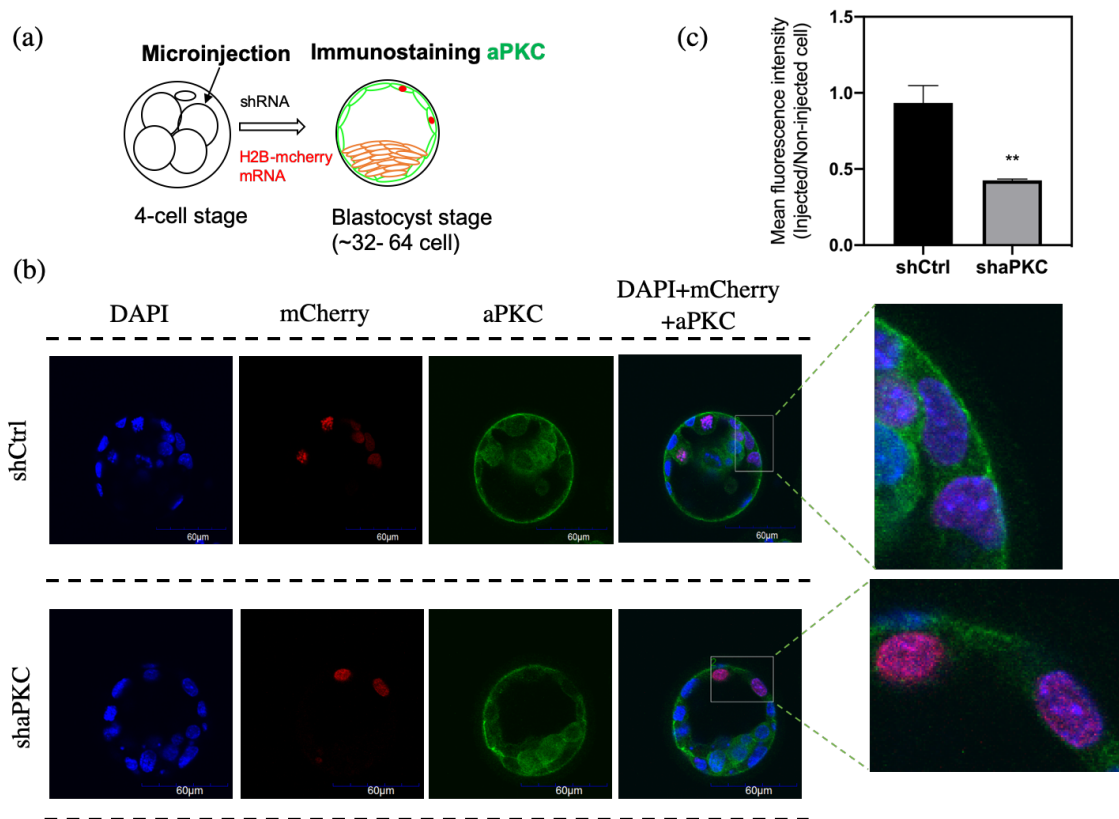


**Figure 3-5.** The aPKC expression was reduced at apical cortex of shaPKC injected progeny cells which were lying outside. (a) Schematic illustration of RNA microinjection experiments in this study. (b) Reduction of aPKC at apical cortex of TE cells. The H2BmCherry mRNA (red) was coinjected with shaPKC or shCtrl. Embryos were immunostained with aPKC  $\lambda$  antibody and the nuclei were stained with DAPI (green). Right panel images are magnified from the square box indicated region of DAPI+mCherry+PKC images. (c) Quantification of aPKC fluorescence intensity in the apical cortex of TE cells of shCtrl and shaPKC injected embryos (n =4 each). \*\*

P= 0.0015, unpaired Student's t-test for comparison of shaPKC against shCtrl injected cells. Bar charts display mean $\pm$ SD.

## Conclusion

In this study, we introduced shRNAs into a single cells of mouse embryo using TatU1A-PS by photo-dependent manner, and also evaluated the effects of aPKC down-regulation on morula and blastocyst stage embryos. Photoinduced RNA internalization by single cell of mouse embryo was demonstrated by using TatU1A-Alexa546/FAM shRNA. The result of photoinduced EGFP knockdown via a single cell RNAi indicated that spatial regulation of gene expression in mouse embryo was achieved by PCDR method. Finally, anti-aPKC shRNA, related to Par6-aPKC polarization, was microinjected into a single cell of four- cell embryos. The aPKC down regulation in early embryos development was studied. In the absence of aPKC, some degree of the injected cells allocated to trophectoderm. It may be because interference of aPKC in a single blastomere before establishing the aPKC polarity at apical domain may not have a significant impact on segregation of TE and ICM cells at blastocyst embryos. Although disruption of aPKC polarization in single blastomere leads to a slight reduction of cell number in morula stage, embryos retained similar cell numbers to control at the blastocyst stage (data not described). These findings are in line with previous report which suggested that aPKC $\lambda$  defective embryos re-establish correct number of inner cells at blastocyst stage (19). It seems aPKC depleted

cells have remaining capacity to segregate as a TE cell. Together, all these data provided that PCDR is a promising approach for the study of regional specific gene function in developmental process of embryos and aPKC polarization is an interested mechanism to be clarified its essential role in embryogenesis. In the future, we will study the effects of aPKC down-regulation by photo-dependent manner, in order to provide a strong evidence that PCDR is a promising approach towards the studies of developmental biology.

## **Materials and Methods**

### **Embryo collection and culture**

Mouse Zygotes were collected from super-ovulated 8- to 12-week-old BDF1 female mice. Females were injected with 5 IU of pregnant mare serum gonadotrophin (PMSG), followed by 5 IU of hCG (human Chorionic Gonadotropin) 48hrs after PMSG. Embryos were obtained by mating the super-ovulated females with BDF1 males. For isolation of fertilized zygotes, super-ovulated females were euthanized 16 hrs post-hCG and zygotes were dissected out of the ampulla in the oviduct. The embryo-cumulus complexes were treated with 300 mg/ml of hyaluronidase to disperse the cumulus cells, washed in MII medium and cultured at 37°C in 5% CO<sub>2</sub>. All animal procedures were performed according to research animal protocols approved by the Animal Care and Use Committee of the Okayama University.

### **Synthetic mRNA preparation**

Histones H2B was amplified by PCR and ligated to EGFP-bearing pcDNA6vector (pcDNA6/Myc-His B; Invitrogen, Carlsbad, CA, USA). d1EGFP mRNA from 12XCSL-d1EGFP plasmid (Addgene Item #47684) and BFP mRNA from pTagBFP-N vector (Cat #FP172) were prepared in vitro as follow. To produce template DNA for mRNA preparation, d1EGFP

or BFP was amplified by PCR from the respective plasmids using following primers: 5` CCG GGT AAT ACG ACT CAC TAT AGG GAC ACA ACT GTG TTT ACT TGC 3` and 5`GATGCTATTGCTTTATTTGTAAC 3` for d1EGFP and 5` CCG GGT AAT ACG ACT CAC TAT AGG TCT ATA TAA GCA GAG CTG G 3` and 5` GTT AAC AAC AAC AAT TGC ATT C 3` for BFP. The sequence for T7 promoter (underline sequence) is added at the 5` end of all forward primers. The PCR was performed using 0.5uM of each primer and 100ng of plasmid in a reaction mixture containing 0.2 mM dNTPs, 12.5 U/mL KOD Dash DNA polymerase (Toyobo, Japan) and 10 µL of 10× buffer, under the following temperature program: 95 °C for 60 s; followed by 25 cycles of 95 °C for 30 s, 58 °C for 2 s, and 73 °C for 30 s. The resultant DNAs were purified by phenol/chloroform extraction and ethanol precipitation. The mRNAs were prepared by in vitro transcription using Invitrogen mMessage mMACHINE T7 transcription kit (# AM1344) and poly (A) tailing with Invitrogen (# AM1350) poly(A) tailing kit according to manufacturer's protocol. The transcribed mRNA was purified by phenol/chloroform extraction and ethanol precipitation.

## Short hairpin RNA preparation

Anti-GFP RNA (shGFP) (5'- GGC UAU GUC UAG GAG UGC ACA UUG CAC UCC GUG CGC UCC UGG ACG UAGCCU U -3') was synthesized by transcription as follows. To generate DNA templates for transcription, primer extension was performed using 1 mM of each primer (5'- CCG GGTAAT ACG ACT CAC TAT AGG CTA TGT CTA GGA GTG CAC ATT GCA C -3' and 5'- AAG GCT ACG TCC AGGAGC GCA CGG AGT GCA ATG TGC ACT CCT AG -3') in a reaction mixture containing 0.2 mM dNTPs, 12.5 U/mL KOD Dash DNA polymerase (Toyobo, Japan) and 10  $\mu$ L of 10 $\times$  buffer, under the following temperature program: 94  $^{\circ}$ C for 120 s; followed by three cycles of 94  $^{\circ}$ C for 30 s, 56  $^{\circ}$ C for 5 s, and 74  $^{\circ}$ C for 20 s. The resultant dsDNA was collected by precipitation with 2-propanol. The transcription reaction was carried out at 37  $^{\circ}$ C for 6 h in a reaction mixture containing 40 mM Tris-HCl (pH 8.0), 20 mM MgCl<sub>2</sub>, 5 mM dithiothreitol (DTT), 10 mM GMP, 2 mM each NTPs, 5 U/ml pyrophosphatase (Sigma-Aldrich, MO, U.S.A.), 20  $\mu$ g/mL T7 RNA polymerase, and 10  $\mu$ g/mL DNA template.

The sequences for anti-aPKC shRNAs: shaPKC-m and shaPKC-L19 are 5'-CCA AAC AUU UCU GGA GAA UCA UUG CAC UCC.GAU UCU CCA GAA AUG UUU GGU U -3' and 5'- UGU ACU GCU AGA CUC

UGA ACA UUG CAC UCC GUU CAG AGU CUA GCA GUA CAU U -  
3', respectively. Primers for preparing transcription templates are as follows:  
5'-CCG GGT AAT ACG ACT CAC TAT ACC AAA CAT TTC TGG AGA  
ATC ATT GCA C -3' and 5' - AAC CAA ACA TTT CTG GAG AAT CGG  
AGT GCA ATG ATT CTC CAG AAA -3' for shaPKC-m and 5' - CCG GGT  
AAT ACG ACT CAC TAT ATG TAC TGC TAG ACT CTG AAC ATT  
GCA C -3' and 5' - AAT GTA CTG CTA GAC TCT GAA CGG AGT GCA  
ATG TTC AGA GTC TAG -3' for shaPKC-L19 were used to generate  
template DNA. A scramble shRNA was used as control shRNA. The  
sequence of shCtrl is 5'-GAG CGA CUA AAC ACA UCA ACA UUG CAC  
UCC GUU GAU GUG UUU AGU CGC UCU U -3'. Following forward and  
reverse primers were used to produce template DNA for shCtrl: 5'-CGA  
AAT TAA TAC GAC TCA CTA TAG AGC GAC TAA ACA CAT CAA  
CAT TGC -3' and 5' - AAG AGC GAC TAA ACA CAT CAA CGG AGT  
GCA ATG TTG ATG TGT TTA GTC GCT CTA -3'. The primer extension  
and *in vitro* transcription were performed as described in shGFP preparation.  
The shRNA transcripts were purified in an 8% denaturing polyacrylamide  
gel. All shRNAs were annealed by incubation at 85 °C for 1 min to remove  
secondary structures, followed by slow annealing (-1 °C/s) to 4 °C.

## **Embryo microinjection**

RNA solution was loaded into glass micropipettes and RNAs were delivered into embryos using piezo-driven micropipette unit (Prime Tech, Japan). For an effective concentration of RNAs, 1:1 ratio of 150 ng/ul shRNAs and/ or 400ng/ul mRNAs were co-injected or injected alone, respectively. Manipulation was carried out in M2 medium containing 5 mg/ml cytochalasin B (Sigma). The volumes injected typically ranged from 2 to 10 pl, which is 1–5% that of the cell.

## **RNA delivery by PCDR method**

TatU1A-PS was prepared as described in materials and methods section of chapter 2. The prepared TatU1A-PS (Alexa 546) (2  $\mu$ M) and shControl or shGFP (400nM) were mixed in T buffer containing 0.1 % of PVA and incubated at 37 °C for 10 min. The embryos were dissolved with enzyme, pronase, to remove zona pellucida and after thoroughly washing 2 times with T buffer (+ 0.1% PVA), zona free embryos were treated for 3h with TatU1A-Alexa546/shRNA complex at 37C, 5% CO<sub>2</sub> incubator. Embryos were washed 2 more times with M2 medium before adhering to the glass base dish mounted with M2 Medium and irradiated under confocal laser scanning microscope (FLUOVIEW FV-1000, Olympus, Japan) as

follow. A single blastomere of four cell-stage embryos was selected by using region of interest tool in software, follow by photobleaching through 40x oil objective lens. A selected single cell was irradiated by a laser at a wavelength of 546 nm. Photobleaching settings were as follow: - type of bleaching: Clip Tornado, laser intensity: 20% or 70%, repetition: 200 or 400 frames.

### **Immunofluorescence staining**

Blastocyst embryos were fixed in 4% paraformaldehyde/PBS for 20 min at room temperature and washed in 1X PBS three times. Embryos were permeabilized in 0.25% Triton X-100/PBS for 20 min at room temperature, followed by washing three times in 1X PBS and transferred to blocking buffer (1% bovine serum albumin/PBS) for 1h at room temperature. Embryos were incubated with primary antibody, mouse monoclonal anti-PKC $\lambda$  (BD Transduction, 1:200 dilution in blocking buffer) at 4C overnight. After washing three times with 1X PBS, embryos were incubated with secondary antibodies: anti-mouse Alexa 488 (ThermoFisher, 1:1000 dilution in PBS or Alexa 568) for 1h at room temperature. Embryos were stained with DAPI (1:200 dilution, in PBS) for 15min. Immunofluorescence images were obtained by confocal laser scanning microscope (FLUOVIEW FV-1000,

Olympus, Japan). Z-stack images were taken at 5 $\mu$ m (step size) intervals with 40x oil objective lens.

### **Quantification of fluorescence intensity**

Fluorescence intensities of cell-contact-free surface (apical surface of the outside cells) of aPKC immunostained embryos were analyzed with Olympus Fluoview software (FV10-ASW.4.2 version). For quantification of aPKC fluorescence intensity, mean fluorescence intensities of outside progeny injected cells were divided by the mean fluorescence intensity of all non-injected outside cells.

## References

1. Tarkowski AK, Wróblewska J. Development of blastomeres of mouse eggs isolated at the 4- and 8-cell stage. *J Embryol Exp Morphol.* 1967.
2. Johnson MH, Pratt HPM, Handyside AH. The Generation and Recognition of Positional Information in the Preimplantation Mouse Embryo. In: *Cellular and Molecular Aspects of Implantation.* ; 1981. doi:10.1007/978-1-4613-3180-3\_5
3. Sasaki H. Position- and polarity-dependent Hippo signaling regulates cell fates in preimplantation mouse embryos. *Semin Cell Dev Biol.* 2015. doi:10.1016/j.semcdb.2015.05.003
4. Yamanaka Y, Ralston A, Stephenson RO, Rossant J. Cell and molecular regulation of the mouse blastocyst. *Dev Dyn.* 2006. doi:10.1002/dvdy.20844
5. Nance J. Getting to know your neighbor: Cell polarization in early embryos. *J Cell Biol.* 2014. doi:10.1083/jcb.201407064
6. Vinot S, Le T, Ohno S, Pawson T, Maro B, Louvet-Vallée S. Asymmetric distribution of PAR proteins in the mouse embryo begins at the 8-cell stage during compaction. *Dev Biol.* 2005.

doi:10.1016/j.ydbio.2005.03.001

7. Johnson MH, Ziomek CA. The foundation of two distinct cell lineages within the mouse morula. *Cell*. 1981. doi:10.1016/0092-8674(81)90502-X
8. Dehghani H, Hahnel AC. Expression profile of protein kinase C isozymes in preimplantation mouse development. *Reproduction*. 2005. doi:10.1530/rep.1.00571
9. Pauken CM, Capco DG. The expression and stage-specific localization of protein kinase C isotypes during mouse preimplantation development. *Dev Biol*. 2000. doi:10.1006/dbio.2000.9763
10. Suzuki A. The PAR-aPKC system: lessons in polarity. *J Cell Sci*. 2006. doi:10.1242/jcs.02898
11. Hirate Y, Hirahara S, Inoue KI, et al. Polarity-dependent distribution of angiotensin localizes hippo signaling in preimplantation embryos. *Curr Biol*. 2013. doi:10.1016/j.cub.2013.05.014
12. Nishioka N, Inoue K ichi, Adachi K, et al. The Hippo Signaling Pathway Components Lats and Yap Pattern Tead4 Activity to Distinguish Mouse Trophectoderm from Inner Cell Mass. *Dev Cell*. 2009. doi:10.1016/j.devcel.2009.02.003
13. Yagi R, Kohn MJ, Karavanova I, et al. Transcription factor TEAD4

- specifies the trophoctoderm lineage at the beginning of mammalian development. *Development*. 2007. doi:10.1242/dev.010223
14. Ralston A, Cox BJ, Nishioka N, et al. Gata3 regulates trophoblast development downstream of Tead4 and in parallel to Cdx2. *Development*. 2010. doi:10.1242/dev.038828
  15. Ciruna BG, Rossant J. Expression of the T-box gene Eomesodermin during early mouse development. *Mech Dev*. 1999. doi:10.1016/S0925-4773(98)00243-3
  16. Niwa H, Toyooka Y, Shimosato D, et al. Interaction between Oct3/4 and Cdx2 determines trophoctoderm differentiation. *Cell*. 2005. doi:10.1016/j.cell.2005.08.040
  17. Chen L, Yabuuchi A, Eminli S, et al. Cross-regulation of the nanog and Cdx2 promoters. *Cell Res*. 2009. doi:10.1038/cr.2009.79
  18. Strumpf D. Cdx2 is required for correct cell fate specification and differentiation of trophoctoderm in the mouse blastocyst. *Development*. 2005. doi:10.1242/dev.01801
  19. Dard N, Le T, Maro B, Louvet-Vallée S. Inactivation of aPKC $\lambda$  reveals a context dependent allocation of cell lineages in preimplantation mouse embryos. *PLoS One*. 2009. doi:10.1371/journal.pone.0007117
  20. Plusa B. Downregulation of Par3 and aPKC function directs cells

towards the ICM in the preimplantation mouse embryo. *J Cell Sci.* 2005.  
doi:10.1242/jcs.01666

21. Zhu M, Leung CY, Shahbazi MN, Zernicka-Goetz M. Actomyosin polarisation through PLC-PKC triggers symmetry breaking of the mouse embryo. *Nat Commun.* 2017. doi:10.1038/s41467-017-00977-8

22. Alarcon VB. Cell Polarity Regulator PARD6B Is Essential for Trophectoderm Formation in the Preimplantation Mouse Embryo1. *Biol Reprod.* 2010. doi:10.1095/biolreprod.110.084400

23. Soloff RS, Katayama C, Lin MY, Feramisco JR, Hedrick SM. Targeted Deletion of Protein Kinase C  $\lambda$  Reveals a Distribution of Functions between the Two Atypical Protein Kinase C Isoforms. *J Immunol.* 2004. doi:10.4049/jimmunol.173.5.3250

24. Ohtsuki T, Miki S, Kobayashi S, et al. The molecular mechanism of photochemical internalization of cell penetrating peptide-cargo-photosensitizer conjugates. *Sci Rep.* 2015;5. doi:10.1038/srep18577

25. Endoh T, Sisido M, Ohtsuki T. Spatial regulation of specific gene expression through photoactivation of RNAi. *J Control Release.* 2009;137(3):241-245. doi:10.1016/j.jconrel.2009.04.015

26. Jedrusik A, Parfitt DE, Guo G, et al. Role of Cdx2 and cell polarity in cell allocation and specification of trophectoderm and inner cell mass in

the mouse embryo. *Genes Dev.* 2008. doi:10.1101/gad.486108

27. Ralston A, Rossant J. Cdx2 acts downstream of cell polarization to cell-autonomously promote trophectoderm fate in the early mouse embryo. *Dev Biol.* 2008. doi:10.1016/j.ydbio.2007.10.054

28. Shiraga K, Soe TH, Matsumoto S, Watanabe K, Ohtsuki T. Red and Near-Infrared Light-Directed Cytosolic Delivery of Two Different RNAs Using Photosensitive RNA Carriers. *Bioconjug Chem.* 2018;29(9):3174-3179. doi:10.1021/acs.bioconjchem.8b00487

## **Acknowledgements**

I wish to express my sincere gratitude to Professor Takashi Ohtsuki for his kind permission to perform this PhD study under his supervision in Biomolecular Engineering Laboratory. I wish to express my sincere thanks for his kindness, patience and encouragement throughout this study. His presence and endless supports are invaluable in planning and accomplishing this study journey. His expertise and constant guidance motivate me for conducting researches and inspire my enthusiasm for lifelong learning.

I would like to thank the thesis reviewing committee and co-supervisors, Professor Hiroshi Tokumitsu and Professor Toru Ide, for their valuable comments and insightful suggestions for my thesis.

I wish to express my sincere gratitude to Assistant Professor Dr. Kazunori Watanabe for his valuable suggestions and the detailed discussions for each experiment in this study. I am also thankful for his kind support and all the help during my study.

I would like to express my sincere thanks to Professor Hiroaki Funahashi for allowing us to do mouse embryo study in his Laboratory.

I am deeply grateful to Associate Professor Dr. Takuya Wakai for his precious time, strong support and valuable suggestions for embryo research.

Without his kind help, I could not imagine the mouse embryo study would be possible.

My sincere thanks go to all member and graduates of Ohtsuki`s laboratory. In particular, I am thankful to Miyoshi San for all of his help and supports during my three years stay in Japan. I greatly appreciate to Shiraga San for her supports, especially, sharing of her laboratory experience and technical know-how. I would like to extend my thanks to Nanjo San, Yuta San, Nawachi San and Inoue San for their assistance and technical support. Due to their friendliness, kindness and warm hospitality like a family, a wonderful memory of doctoral study at Ohtsuki`s Lab will remain forever in my heart.

I also would like to express my gratitude to my parent, U Kyin Soe and Daw Win Ye for their love, support and encouragement throughout my life. Last but not the least, special thanks to my beloved wife, Sandar Aung for always being ready to support me and giving me strength and motivation to achieve my goals. Without her love and understanding, I could not have made this study journey.

I gratefully acknowledge the funding received towards my PhD from MEXT (Ministry of Education, Culture, Sports, Science and Technology) Japan.

## List of Publications

(1) Relation of photochemical internalization to heat, pH, and Ca<sup>2+</sup> ions

Tet Htut Soe, Tomotaka Nanjo, Kazunori Watanabe, and Takashi Ohtsuki

Photochemistry and Photobiology. doi:[10.1111/php.13146](https://doi.org/10.1111/php.13146).

(2) Red and near-infrared light-directed cytosolic delivery of two different RNAs using photosensitive RNA carriers

Kaori Shiraga, Tet Htut Soe, Sho Matsumoto, Kazunori Watanabe,

and Takashi Ohtsuki

Bioconjugate chemistry, 29, 3174–3179 (2018).

## Oral and Poster Presentation

(1) Mechanism and application of photoinduced cytosolic dispersion of RNA (PCDR) method (oral presentation at symposium)

Tet Htut Soe, Takashi Ohtsuki, and Kazunori Watanabe

The 56<sup>th</sup> Annual Meeting of the Biophysical Society of Japan, Vol 58

(Okayama, 2018.Sept 15-17)